Eur. Phys. J. C manuscript No.
(will be inserted by the editor)

Development of ^{100}Mo-containing scintillating bolometers for a high-sensitivity neutrinoless double-beta decay search

E. Armengaud[1], C. Augier[2], A.S. Barabash[3], J.W. Beeman[4], T.B. Bekker[5], F. Bellini[6,7], A. Benoît[8], L. Bergé[9], T. Bergmann[10], J. Billard[2], R.S. Boiko[11], A. Broniatowski[9,12], V. Brudanin[13], P. Camus[8], S. Capelli[14,15], L. Cardani[7], N. Casali[7], A. Cazes[2], M. Chapellier[9], F. Charlieux[2], D.M. Chernyak[11,33], M. de Combarieu[16], N. Coron[17], F.A. Danevich[11], I. Dafinei[7], M. De Jesus[2], L. Devoyon[18], S. Di Domizio[19,20], L. Dumoulin[9], K. Eitel[21], C. Enss[22], F. Ferroni[6,7], A. Fleischmann[22], N. Foerster[12], J. Gascon[2], L. Gastaldo[22], L. Gironi[14,15], A. Giuliani[9,23], V.D. Grigorieva[24], M. Gros[1], L. Hehn[21,34], S. Hervé[1], V. Humbert[9], N.V. Ivannikova[24], I.M. Ivanov[24], Y. Jin[25], A. Juillard[2], M. Kleifges[10], V.V. Kobychev[11], S.I. Konovalov[3], F. Koskas[18], V. Kozlov[12], H. Kraus[26], V.A. Kudryavtsev[27], M. Laubenstein[28], H. Le Sueur[9], M. Loidl[29], P. Magnier[1], E.P. Makarov[24], M. Mancuso[9,23,35], P. de Marcillac[9], S. Marnieros[9], C. Marrache-Kikuchi[9], S. Nagorny[28,30], X-F. Navick[1], M.O. Nikolaichuk[11], C. Nones[1], V. Novati[9], E. Olivieri[9], P. Pari[16], L. Pattavina[28], M. Pavan[14,15], B. Paul[1], Y. Penichot[1], G. Pessina[14,15], G. Piperno[31], S. Pirro[28], O. Plantevin[9], D.V. Poda[a,9,11], E. Queguiner[2], T. Redon[17], M. Rodrigues[29], S. Rozov[13], C. Rusconi[15], V. Sanglard[2], K. Schäffner[28], S. Scorza[12,36], V.N. Shlegel[24], B. Siebenborn[21], O. Strazzer[18], D. Tcherniakhovski[10], C. Tomei[7], V.I. Tretyak[11], V.I. Umatov[3], L. Vagneron[2], Ya.V. Vasiliev[24], M. Velazquez[32], M. Vignati[7], M. Weber[10], E. Yakushev[13], A.S. Zolotarova[1]

arXiv:1704.01758v1 [physics.ins-det] 6 Apr 2017

[1] IRFU, CEA, Université Paris-Saclay, F-91191 Gif-sur-Yvette, France
[2]Univ Lyon, Université Lyon 1, CNRS/IN2P3, IPN-Lyon, F-69622, Villeurbanne, France
[3]National Research Centre Kurchatov Institute, Institute of Theoretical and Experimental Physics, 117218 Moscow, Russia
[4]Lawrence Berkeley National Laboratory, Berkeley, California 94720, USA
[5]V.S. Sobolev Institute of Geology and Mineralogy of the Siberian Branch of the RAS, 630090 Novosibirsk, Russia
[6]Dipartimento di Fisica, Sapienza Università di Roma, P.le Aldo Moro 2, I-00185, Rome, Italy
[7]INFN, Sezione di Roma, P.le Aldo Moro 2, I-00185, Rome, Italy
[8]CNRS-Néel, 38042 Grenoble Cedex 9, France
[9]CSNSM, Univ. Paris-Sud, CNRS/IN2P3, Université Paris-Saclay, 91405 Orsay, France
[10]Karlsruhe Institute of Technology, Institut für Prozessdatenverarbeitung und Elektronik, 76021 Karlsruhe, Germany
[11]Institute for Nuclear Research, 03028 Kyiv, Ukraine
[12]Karlsruhe Institute of Technology, Institut für Experimentelle Kernphysik, 76128 Karlsruhe, Germany
[13]Laboratory of Nuclear Problems, JINR, 141980 Dubna, Moscow region, Russia
[14]Dipartimento di Fisica, Università di Milano Bicocca, I-20126 Milano, Italy
[15]INFN, Sezione di Milano Bicocca, I-20126 Milano, Italy
[16]IRAMIS, CEA, Université Paris-Saclay, F-91191 Gif-sur-Yvette, France
[17]IAS, CNRS, Université Paris-Sud, 91405 Orsay, France
[18]Orphée, CEA, Université Paris-Saclay, F-91191 Gif-sur-Yvette, France
[19]Dipartimento di Fisica, Università di Genova, I-16146 Genova, Italy
[20]INFN Sezione di Genova, I-16146 Genova, Italy
[21]Karlsruhe Institute of Technology, Institut für Kernphysik, 76021 Karlsruhe, Germany
[22]Kirchhoff Institute for Physics, Heidelberg University, D-69120 Heidelberg, Germany
[23]DISAT, Università dell'Insubria, 22100 Como, Italy
[24]Nikolaev Institute of Inorganic Chemistry, 630090 Novosibirsk, Russia
[25]Laboratoire de Photonique et de Nanostructures, CNRS, Route de Nozay, 91460 Marcoussis, France
[26]University of Oxford, Department of Physics, Oxford OX1 3RH, UK
[27]Department of Physics and Astronomy, University of Sheffield, Hounsfield Road, Sheffield S3 7RH, UK
[28]INFN, Laboratori Nazionali del Gran Sasso, I-67100 Assergi (AQ), Italy
[29]CEA Saclay, LIST, Laboratoire National Henri Becquerel, 91191 Gif-Sur-Yvette Cedex, France
[30]INFN, Gran Sasso Science Institute, I-67100 L'Aquila, Italy
[31]INFN, Laboratori Nazionali di Frascati, I-00044 Frascati (Roma), Italy
[32]ICMCB, CNRS, Université de Bordeaux, 33608 Pessac Cedex, France
[33]Presently at Kavli Institute for the Physics and Mathematics of the Universe (WPI), The University of Tokyo Institutes for Advanced Study, The University of Tokyo, Kashiwa, Chiba, Japan
[34]Presently at Lawrence Berkeley National Laboratory, Berkeley, CA, USA
[35]Presently at Max-Planck-Institut für Physik, Munich, Germany
[36]Presently at SNOLAB, Lively, ON, Canada

Received: date / Accepted: date

Abstract We report recent achievements in the development of scintillating bolometers to search for neutrinoless double-beta decay of ^{100}Mo. The presented results have been obtained in the framework of the LUMINEU, LUCIFER and EDELWEISS collaborations, and are now part of the R&D activities towards CUPID (CUORE Update with Particle IDentification), a proposed next-generation double-beta decay experiment based on the CUORE experience. We have developed a technology for the production of large mass (∼1 kg), high optical quality, radiopure zinc and lithium molybdate crystal scintillators ($ZnMoO_4$ and Li_2MoO_4,

[a]e-mail: denys.poda@csnsm.in2p3.fr

respectively) from deeply purified natural and ^{100}Mo-enriched molybdenum. The procedure is applied for a routine production of enriched crystals. Furthermore, the technology of a single detector module consisting of a large-volume ($\sim$ 100 cm^3) $Zn^{100}MoO_4$ and $Li_2{}^{100}MoO_4$ scintillating bolometer has been established, demonstrating performance and radiopurity that are close to satisfy the demands of CUPID. In particular, the FWHM energy resolution of the detectors at 2615 keV — near the Q-value of the double-beta transition of ^{100}Mo (3034 keV) — is $\approx$ 4–10 keV. The achieved rejection of α-induced dominant background above 2.6 MeV is at the level of more than 99.9%. The bulk activity of ^{232}Th (^{228}Th) and ^{226}Ra in the crystals is below 10 μBq/kg. Both crystallization and detector technologies favor Li_2MoO_4, which was selected as a main element for the realization of a CUPID demonstrator (CUPID-0/Mo) with $\sim$7 kg of ^{100}Mo.

Keywords Double-beta decay · Scintillating bolometer · Zinc molybdate · Lithium molybdate · Enriched ^{100}Mo

PACS 29.40.Mc Scintillation detectors · 23.40.-s Double-β decay

1 Introduction

Neutrinoless double-beta ($0\nu2\beta$) decay, a hypothetical, very rare, nuclear transition consists in a transformation of an even-even nucleus into a lighter isobar containing two more protons and accompanied by the emission of two electrons and no other particles, with a change of the total lepton number by two units: $(A, Z) \rightarrow (A, Z + 2) + 2e^-$ (e.g. see Ref. [1]). This transition is possible for 35 nuclei [2] and has never been detected. The observation of $0\nu2\beta$ decay would have profound implications for our understanding of nature, proving that neutrinos are their own antiparticles (Majorana fermions) and offering also a clue for the creation of matter abundance in the primordial universe (see recent reviews [1,3] and references therein). It is however to remark that this process is much more than a neutrino-physics experiment. It is a powerful, inclusive test of lepton number violation. Non-conservation of the total lepton number is as important as baryon number violation and naturally incorporated by theories beyond the Standard Model (SM). The current best limits on $0\nu2\beta$ decay are in the range of 10^{24}–10^{26} yr [1,4]. The SM process, two neutrino double-beta ($2\nu2\beta$) decay, which implies also the emission of two electron antineutrinos, is the rarest nuclear decay and has been observed in 11 nuclei with half-lives in the range of 10^{18}–10^{24} yr [5].

There are a number of proposed next-generation $0\nu2\beta$ decay experiments, based on upgrades of the most promising current technologies (e.g. see Refs. [1, 6,7,8,9]). The goal of these future searches is to improve by up to two orders of magnitude the present best limits on the half-life, with a sensitivity to the absolute neutrino mass scale at the level of 10–20 meV, covering the so-called inverted hierarchy region of the neutrino mass pattern. The bolometric technique is one of the most powerful methods to investigate $0\nu2\beta$ decay. The Cryogenic Underground Observatory for Rare Events (CUORE) [10], which studies the candidate ^{130}Te, is by far the most important bolometric $0\nu2\beta$ decay experiment and even its precursors Cuoricino and CUORE-0 are ones of the most sensitive current searches [1]. CUORE is now in pre-operation phase in the Gran Sasso National Laboratories (Italy) and will be in operation for several years. A large group of interest is

now proposing a next-generation bolometric experiment, CUORE Upgrade with Particle ID (CUPID) [11,12], to follow CUORE after the completion of its physics program. CUPID aims to improve the sensitivity by two orders of magnitude over CUORE. The nuclei ^{130}Te, ^{100}Mo, ^{82}Se and ^{116}Cd are the $0\nu2\beta$ candidates considered for CUPID. A down-selection of the CUPID technology, isotope and material is foreseen in 2018/2019.

Scintillating bolometers, the devices used in the present work, are amongst the most powerful nuclear detectors for the conduction of sensitive $0\nu2\beta$ decay searches, as they offer high detection efficiency, excellent energy resolution (at the level of $\sim$0.1%), efficient $\alpha/\gamma(\beta)$ particle separation and potentially low intrinsic background [9,13,14]. The ^{100}Mo isotope is one of the most promising $0\nu2\beta$ candidates, since its $0\nu2\beta$ signal is expected at $Q_{\beta\beta} = 3034$ keV [15] (Q-value of the transition), while environmental γ background mainly ends at 2615 keV. The candidate is embedded in $ZnMoO_4$ and Li_2MoO_4 crystals, working as bolometers but being also low temperature scintillators. An auxiliary bolometer, consisting of a thin Ge wafer, faces each Mo-containing crystal in order to detect the scintillation light. The energy region above $\sim$2.6 MeV is dominated by events produced by radioactive contamination of surfaces, especially α particles (as shown by the results of Cuoricino [16] and CUORE-0 [17]). Since the scintillation signal from alpha particles is typically quenched in comparison to the $\gamma(\beta)$ light yield at equal deposited energy [18], while the bolometric thermal response is substantially equivalent, the simultaneous detection of light and heat represent a powerful tool to reject background efficiently [7,8,9,13].

Preliminary results have been achieved in the past with Mo-containing bolometers — using molybdenum with natural isotopic composition — in the Gran Sasso underground laboratory in Italy [8,19,20,21,22], in the Modane underground laboratory in France [23,24,25,26] and in an aboveground cryogenic laboratory located at CSNSM (Orsay, France) [27,28,29,30,31,32], where also a first small ^{100}Mo-enriched $ZnMoO_4$ two-detector array has been tested recently [33]. Most of these R&D activities were conducted in the framework of the scintillating-bolometer research programs of LUCIFER — focused on ZnSe for the $0\nu2\beta$ decay candidate ^{82}Se but involving also $ZnMoO_4$ — and of LUMINEU, dedicated to the investigation of ^{100}Mo. The present work represents a crucial step forward in the development of radiopure scintillating bolometers based on $ZnMoO_4$ and Li_2MoO_4 crystals grown from ^{100}Mo-enriched molybdenum. A protocol for crystal growth was developed, and several prototypes were tested showing excellent energy resolution, efficient $\alpha/\gamma(\beta)$ rejection power and remarkable radiopurity. The results described here prove in particular that the Li_2MoO_4 technology is mature to carry out a pilot experiment on a several-kilogram scale, and they provide essential elements for the choice of the CUPID technique, by clarifying the merits and the drawbacks of the ^{100}Mo option.

2 R&D of natural and ^{100}Mo-enriched zinc and lithium molybdates

2.1 Development of $ZnMoO_4$ and $Zn^{100}MoO_4$ crystal scintillators

Besides high scintillation yield and good optical properties, there are two strong specific requirements for Mo-containing crystal scintillators to be applied in $0\nu2\beta$

decay experiments: as-low-as-possible levels of radioactive contamination and losses of high cost enriched molybdenum in the purification-crystallization chain. Therefore, an extensive R&D of $ZnMoO_4$ crystal scintillators has been performed by LUMINEU. Below, we briefly overview the main achievements, while all details can be found in Refs. [23,24,25,26,30,31,33].

LUMINEU developed a dedicated protocol for molybdenum purification consisting in the sublimation of molybdenum oxide (MoO_3) in vacuum and additional recrystallization of ammonium molybdate from aqueous solutions [30].

The low-thermal-gradient Czochralski (LTG Cz) technique [34,35], developed at the Nikolaev Institute of Inorganic Chemistry (NIIC, Novosibirsk, Russia), has been chosen for $ZnMoO_4$ crystal production. This method enabled the growth of a large-mass (∼1.5 kg) colorless $ZnMoO_4$ boule with a high yield (∼80% of initial charge), using deeply purified materials [30]. Several scintillating elements with high optical quality and large volume (with sizes up to ⌀35×40 mm), were produced and successfully tested above ground as scintillating bolometers showing high performance and radiopurity [30].

A further progress was achieved by applying a double crystallization protocol to grow a ∼ 1.0 kg $ZnMoO_4$ crystal boule of improved quality. Two transparent scintillating elements (see Table 1) were produced for the low-temperature tests [23,24, 25,26]. The crystal size ⌀50×40 mm was chosen by the LUMINEU collaboration so that the single detection module was compatible with the EDELWEISS set-up (see Sec. 3.1.1). Also, it is worth to stress that the volume of ^{100}Mo-containing bolometers should not be too large to avoid a significant impact on background from random coincidences of the $2\nu2\beta$ decay events of ^{100}Mo [36,37].

Table 1 Zinc and lithium molybdate crystal scintillators produced by the LTG Cz method from molybdenum with natural isotopic composition and enriched in ^{100}Mo. All crystals were grown from a molybdenum compound purified by single or double sublimation and double recrystallization. A Li_2CO_3 compound supplied by NRMP (see the text) was used to produce all Li-containing scintillators, except LMO-3 (produced from Alfa Aesar Li_2CO_3). Position in the crystal boule is given for those samples cut from the same boule

Scintillator	Molybdenum sublimation	Boule crystallization	Crystal ID	Position in boule	Size (⌀×h mm)	Mass (g)
$ZnMoO_4$	Single	Double	ZMO-t	top	50×40	336
			ZMO-b	bottom	50×40	334
$Zn^{100}MoO_4$	Double	Single	enrZMO-t	top	60×40	379
			enrZMO-b	bottom	60×40	382
Li_2MoO_4	Single	Single	LMO-1	–	40×40	151
	Single	Double	LMO-2	–	50×40	241
	Single	Single	LMO-3	–	50×40	242
$Li_2{}^{100}MoO_4$	Double	Triple	enrLMO-t	top	44×40	186
			enrLMO-b	bottom	44×44	204
	Double	Double	enrLMO-2t	top	44×46	213
			enrLMO-2b	bottom	44×44	207

A first ^{100}Mo-enriched $Zn^{100}MoO_4$ crystal scintillator (with a mass of ∼ 0.17 kg, 99.5% of ^{100}Mo) was developed and tested [33]. The high crystal yield (84%) and the low irrecoverable losses of the enriched material (∼4%) together with encour-

aging results of the aboveground bolometric test of two 60-g $Zn^{100}MoO_4$ detectors represent an important milestone of this R&D.

Further progress in the $ZnMoO_4$ development was achieved by adding a small amount of tungsten oxide (up to ∼0.5% weight) to the $ZnMoO_4$ compound in order to stabilize the melt in the ZnO-MoO_3 system [31]. Several high quality ∼0.15-kg crystal boules were grown. A low-temperature test with two scintillating elements of the same size (⌀20×40 mm) — one with stoichiometric composition and the other one doped by W — confirmed that the excess of tungsten does not affect the bolometric properties of $ZnMoO_4$ crystals [31].

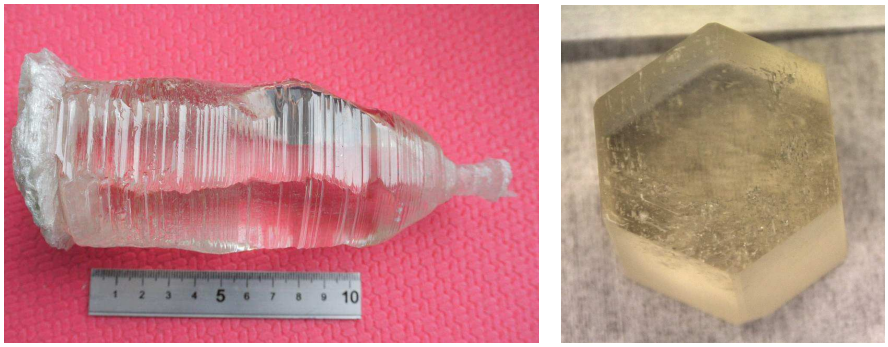

(a) (b)

Fig. 1 Photographs of the ∼1.4 kg boule of $Zn^{100}MoO_4$ crystal (a) grown by the low-thermal gradient Czochralski method from ^{100}Mo-enriched molybdenum and the ∼0.38 kg $Zn^{100}MoO_4$ scintillation element (b) produced from the top part of the boule

A large-mass $Zn^{100}MoO_4$ crystal boule (mass of ∼ 1.4 kg, isotopic concentration of ^{100}Mo ∼ 99%) was grown [25,26] and two hexagonal-shaped scintillation elements were produced for the bolometric measurements (see Table 1 and Fig. 1). This shape was chosen to minimize the material losses and to get an improved light output [38]. There is still room to improve the crystal quality, because the $Zn^{100}MoO_4$ boule exhibits a faceted structure and contains inclusions, mainly in the bottom part.

2.2 Development of Li_2MoO_4 and $Li_2{}^{100}MoO_4$ crystal scintillators

Because of some experienced difficulties with the $ZnMoO_4$ crystallization process, the LUMINEU collaboration initiated an R&D for the production of lithium molybdate (Li_2MoO_4) [39]. This scintillator looks a promising detector thanks to the low melting point (705 °C; see the material properties in Ref. [32]), comparatively easier crystal growth [40,41,42], higher concentration of molybdenum (55% weight), promising scintillating-bolometer performance [22], and considerably high intrinsic radiopurity [22] (except for ^{40}K [40]). It should be stressed that lithium does not contain long-lived radioactive isotopes but it has a high thermal-neutron

cross section (^{6}Li, $\sim$ 940 barns [43]). Nevertheless, neutron absorption leads to the reaction ^{6}Li(n,t)α, which gives α+t events (Q-value is 4784 keV [43]) easily separated from $\gamma(\beta)$ events [22]. Finally, a possible cosmogenic activation of lithium is expected to be much less valuable than that of zinc.

First high quality 0.1–0.4 kg Li_2MoO_4 crystal boules were grown by the LTG Cz with a high yield (more than 80% of initial charge) by using deeply purified molybdenum oxide [30] and high purity lithium carbonate (Li_2CO_3, Novosibirsk rare metals plant, NRMP, Novosibirsk, Russia) [32]. Thanks to the low melting point, the Li_2MoO_4 crystals were grown with very low irrecoverable losses of molybdenum, less than 0.1% (one can compare with 0.6% in case of $ZnMoO_4$ [33]). A large Li_2MoO_4 scintillation element (LMO-1, see Table 1), $\approx$4.6 times heavier than the largest previously tested sample [22], was cut from the crystal boule and tested at low-temperatures ([32] and the present work).

An activity approximately of 60 mBq/kg of ^{40}K was detected in the LMO-1 crystal in an underground measurement (see Sec. 5.1.1). Despite the low Q_β of ^{40}K, random coincidences of ^{40}K and $2\nu2\beta$ events can produce background in the ragion of interest (ROI; e.g. FWHM wide centered at $Q_{\beta\beta}$) [37]. Contamination of a $Li_2{}^{100}MoO_4$ detector with dimension $\oslash 50 \times 40$ mm on the level of $\sim$57 mBq/kg provides the same background counting rate in the ROI as random coincidences of the $2\nu2\beta$ events of ^{100}Mo. Therefore, the potassium contamination should be reduced at least by one order of magnitude.

An R&D was performed aiming at the production of radiopure Li_2MoO_4 crystal scintillators. The R&D includes the radioactive screening and selection of commercial lithium carbonate samples, investigating of segregation of radioactive elements in the crystallization process, and developing of Li_2CO_3 purification.

Three samples of high purity lithium carbonate were measured by HPGe spectrometry at the STELLA facility of Gran Sasso underground laboratory (Italy): 1) 99.99% purity grade powder produced by NRMP; 2) 99.998% lithium carbonate by Puratronic (Alfa Aesar GmbH & Co KG, France); 3) 99.99% raw material by Sigma-Aldrich (USA). The results are given in Table 2. The lithium carbonate produced by NRMP is the material of highest radiopurity. Due to high ^{40}K contamination in the Sigma-Aldrich material, it was rejected for the further investigation.

Table 2 Radiopurity of Li_2CO_3 compounds and Li_2MoO_4 crystals (errors in parenthesis are given at 68% C.L., upper limits — at 95% C.L.). The measurements of radioactive contamination in the Li_2CO_3 samples were done by low background HPGe γ spectrometry, while the bolometric technique was used to investigate the Li_2MoO_4 crystals' contamination

Chain	**Nuclide**	**Activity (mBq/kg)**					
		Powder NRMP	Crystal LMO-1	Crystal LMO-2	Powder Alfa Aesar	Crystal LMO-3	Powder Sigma-Aldrich
^{232}Th	^{232}Th	–	$\leq$ 0.023	$\leq$ 0.026	–	$\leq$ 0.024	–
	^{228}Ra	$\leq$ 2.9	–	–	$\leq$ 14	–	16(8)
	^{228}Th	$\leq$ 3.7	$\leq$ 0.023	$\leq$ 0.026	12(4)	$\leq$ 0.024	13(4)
^{238}U	^{226}Ra	$\leq$ 3.3	$\leq$ 0.051	$\leq$ 0.044	705(30)	0.13(2)	53(6)
	^{40}K	$\leq$ 42	62(2)	$\leq$ 12	$\leq$ 42	$\leq$ 3.3	210(70)

Li_2MoO_4 crystals with up to 55 mm in diameter were grown by the LTG Cz method in a platinum crucible 68 mm in diameter [39]. The crucible was provided with a cone lid having a pipe socket through which passed the pull rod with the crystal holder. A 0.36 kg Li_2MoO_4 crystal boule was grown by double crystallization from NRMP Li_2CO_3 compound, while another one (0.61 kg) was grown by single crystallization from Alfa Aesar Li_2CO_3 powder. Two identical samples were cut from these boules (LMO-2 and LMO-3, respectively; see Table 1). The bolometric test of the detectors gives only upper limits on the potassium concentration at the level of a few mBq/kg of ^{40}K (see Table 2 and Sec. 5.1.1). The data for the LMO-2 crystal indicate segregation of potassium in the crystal growth process by at least one order of magnitude. Furthermore, segregation of thorium and radium is even more efficient as one can see by comparing the radioactive contamination of the LMO-3 crystal and the Li_2CO_3 powder used for the crystal growth.

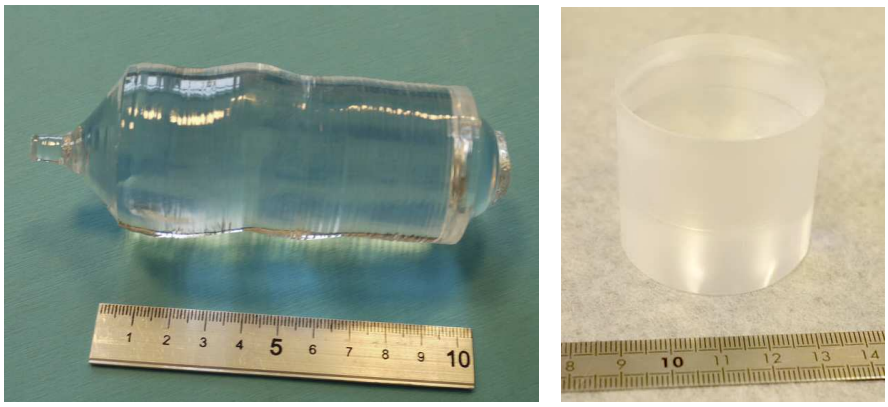

(a) (b)

Fig. 2 (a) A photograph of the first $\sim$ 0.5 kg boule of $Li_2{}^{100}MoO_4$ crystal grown from ^{100}Mo-enriched molybdenum by the low-thermal gradient Czochralski technique. (b) A photograph of the $\sim$0.2 kg $Li_2{}^{100}MoO_4$ scintillation element cut from the top part of the crystal boule

A first ^{100}Mo-enriched (96.9% of ^{100}Mo) crystal boule with mass of $\sim$ 0.5 kg was grown by LTG Cz in the beginning of 2016 (see Fig. 2(a)). The crystal was produced by a triple crystallization due to an accident which happened during the second crystal growth process. Two similar size $Li_2{}^{100}MoO_4$ scintillation elements (see Table 1 and Fig. 2(b)) were cut from the boule and used for the bolometric tests described in the next Section. The second $\sim$ 0.6 kg $Li_2{}^{100}MoO_4$ crystal boule was grown by double crystallization at the end of May 2016 (see Fig. 4 in [39]) and two cylindrical elements were produced (see Table 1). All these $Li_2{}^{100}MoO_4$ elements are presently used in the four-bolometers array test in the EDELWEISS set-up (France).

3 Underground tests of Mo-containing scintillating bolometers

3.1 Underground cryogenic facilities

3.1.1 EDELWEISS-III set-up

The EDELWEISS-III cryogenic set-up is located in the Modane underground laboratory (LSM, France). The 1.7 km mean rock overburden provides the 4.8 km of water equivalent (km w.e.) shield against cosmic rays. The set-up consists of a reversed-geometry dilution refrigerator with a large experimental volume (50 L) that can host up to 48 single detector modules with a copper holder size of $\approx \oslash 80\times 60$ mm each. The cryostat hosting the refrigerator is provided with passive and active shielding. All the set-up is made with low-radioactivity materials. A cold electronics — featuring AC bolometer bias modulated at a frequency of up to 1 kHz — and 16 bits ADC boards are used to acquire the data with a sampling frequency of 100 kSPS. The data of scintillating bolometers were on-line triggered by heat channels; once a detector fires, the data of all operating detectors are recorded. A ≈2-sec-long waveform contains a baseline in the first half of the window and a triggered signal in the second half. All details about the set-up, cryogenics and electronics can be found in Refs. [23, 44, 45].

The EDELWEISS set-up was conceived to perform direct dark-matter searches with the help of massive heat-ionization bolometers, which imply the investigation of the low energy region (below tens of keV). Thus, some features of the set-up are not perfectly suitable to the scintillating-bolometer technology and $0\nu 2\beta$ searches (the ROI at few MeV):

- The mechanical decoupling system is adapted to the operation of tightly held massive EDELWEISS detectors, and not to scintillating bolometers;
- Difficulties in the operation of high resistance (> 10 MΩ at the working point, at ∼20 mK) Neutron Transmutation Doped (NTD) Ge temperature sensors [46] with AC bias (e.g. unbalanced compensation of non linearities of the differentiated triangular wave applied for NTD excitation, see details in [45, 47]);
- Absence of a set-up to periodically inject temperature pulses into the bolometers through a heater for the stabilization of their thermal response [48];
- No procedure foreseen for the regular calibration at high energy. A periodical calibration is only available with a ^{133}Ba source (γ's with energies below 0.4 MeV) automatically inserted through the lead shield;
- Prohibition of the in-situ use of ^{55}Fe sources for the light detectors calibration.

However, four years' experience of running scintillating bolometers in this set-up helped us to mitigate the aforementioned issues, with the following measures:

- Operation of scintillating bolometers in a mechanically-isolated suspended tower (since 2016);
- Use of mainly low resistance (~ 1 MΩ at the working point) NTD Ge sensors (since 2015);
- Use of a dedicated pulser system (since 2015);
- Use of a ^{232}Th γ source made of thoriated tungsten wires (since 2014). Unfortunately, the source insertion requires lead shield opening which is not supposed to be done frequently (in practice, only once per each cryogenic campaign).

3.1.2 CUPID R&D set-up

The CUPID R&D cryogenic set-up is located deep underground (3.6 km w.e) at the Gran Sasso National Laboratories (LNGS, Italy) in the Hall C. The cryostat (Oxford TL200 ^{3}He/^{4}He dilution refrigerator) is able to reach 7 mK base temperature. The available experimental volume is $\sim$ 8 L. The cryostat is provided with shields for γ and neutron flux attenuation and an anti-radon system. An important feature of the set-up is a two-stage damping system [49] which decouples mechanically the detectors from the mixing chamber. The Front End Electronics comprises an amplification stage, a six-pole anti-aliasing active Bessel filter (120 dB/decade) and a 18 bits NI-PXI-6284 ADC board operating at the chosen sampling frequency. The bolometers are DC biased. Details of the cryogenic system and electronics are in Refs. [49,50,51]. The calibration of heat detectors is periodically done with a movable ^{228}Th source (^{40}K and ^{137}Cs are also available) deployed between the dewar housing the cryostat and the external lead shield. In addition, heat detectors can be faced by a smeared ^{238}U α source in order to produce α particles with energies below 4 MeV. For the calibration of light detectors, a permanent ^{55}Fe X-ray source is fixed on the light-detector holders.

Heat-light double read-out is implemented in the following way. For each software-generated trigger, 2000 (75) ms long waveforms for the heat (light) detectors are acquired. When the heat channel trigger fires, the simultaneous light channel waveform is recorded irrespectively of its trigger. Random events, not containing triggered pulses, are saved for noise characterization. In addition, streaming data are recorded along with the triggered data.

3.2 Mo-containing scintillating bolometers

The detectors were fabricated from the crystal scintillators listed in Table 1 and assembled according to either LUMINEU or LUCIFER standard schemes (see Table 3). The mechanical structure and the optical coupling to the crystal scintillators are designed to optimize the heat flow through the sensors and to maximize the light collection. The standard adopted by LUMINEU for the EDELWEISS-III set-up implies the use of a dedicated copper holder where the crystal scintillator is fixed by means of L- and S-shaped PTFE clamps [23,24,25]. The holder is completely covered internally by a reflector to improve the scintillation-light collection. For the prototype of the LUMINEU suspended tower, shown in Fig. 3, the holders were slightly modified to make an array structure able to pass through the holes in the copper plates of the EDELWEISS set-up. In case of the LUCIFER R&D standard, the crystal is fixed to a copper frame by S-shaped PTFE pieces and copper columns, as well as side-surrounded by a plastic reflective film (e.g. see in [8]). This frame is thermally anchored to the mixing chamber of the dilution refrigerator.

Each scintillating crystal was instrumented by one or two epoxy-glued NTD Ge temperature sensors. The thermal link to the bath was provided by Au bonding wires which give also the electrical connection with the NTD Ge sensors. The NTD Ge thermistors, biased with a constant current, act as temperature-voltage transducers. In addition, each bolometer was supplied with a small Si heater carrying a heavily-doped Si:P meander [52], through which a constant Joule power was peri-

Table 3 The main construction elements of Mo-containing detectors studied in the present work. Three types of reflectors were used: Radiant Mirror Film (RMF) VM2000/VM2002 and Enhanced Specular Reflector (ESR) film by 3M^{TM}and a thin silver layer (Ag) deposited on the holder. High and low resistivity NTD Ge sensors are denoted as HR and LR, respectively. The masses of all the used sensors are ≈50 mg. The enrZMO-t, enrZMO-b, and LMO-2 detectors were also equipped with a smeared ^{238}U α source

Standard	Crystal ID	Support		Reflector	NTD sensor	
		Copper	PTFE		No.1	No.2
LUMINEU	ZMO-t	Holder	L- and S-shaped	RMF	HR	HR
	ZMO-b				HR	LR
	LMO-1				HR	–
	LMO-3			Ag	LR	–
LUMINEU (tower)	ZMO-b	Holder	L- and S-shaped	ESR	LR	–
	enrLMO-t				LR	–
LUCIFER	enrZMO-t	Plate, columns	S-shaped	ESR	LR	LR
	enrZMO-b				LR	LR
	LMO-2				LR	LR
	enrLMO-b				HR	HR

odically injected to stabilize the bolometer response over temperature fluctuations [48, 52].

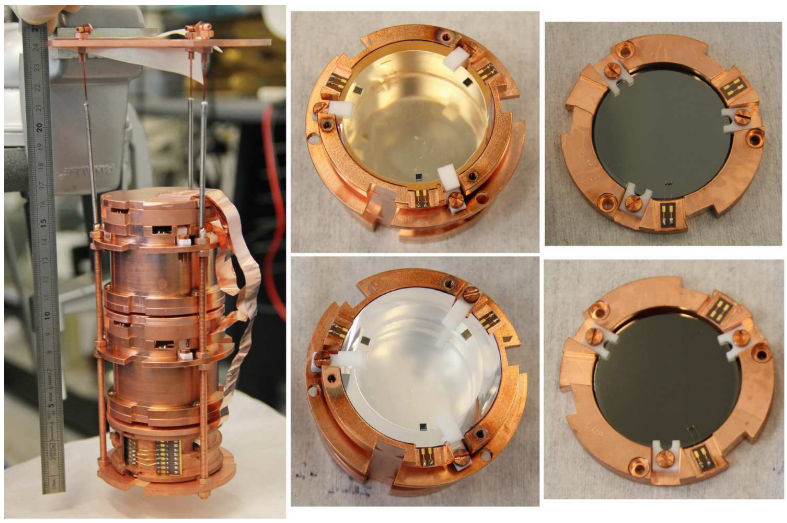

Fig. 3 Photographs of a three-spring suspended tower (first column) and two LUMINEU scintillating bolometers (second column): the 334 g $ZnMoO_4$ (top) and the 186 g $Li_2{}^{100}MoO_4$ (bottom) bolometers together with two identical Ge light detectors (third column). A third detector of the tower (bottom in the left photo, not shown in details) is a 0.2 kg Ge bolometer

Thin bolometric detectors (light detectors, see Table 4) were coupled to the scintillating crystals to register the scintillation light. All of them are based on high purity Ge wafers which are, in most cases, fixed into the copper frame by PTFE clamps. Part of light detectors were constructed according to the LUMINEU standard [53], which also implies the deposition of a 70 nm SiO antireflecting layer

on one surface of the Ge waver to increase light absorption [54]. Another type of similar-performance light detectors used in the present study was developed by the LUCIFER group [55]; one bolometer was assembled according to CUPID-0 mounting standard [56]. The last type of the used light detectors is the state-of-the-art optical bolometers developed at IAS (Orsay, France) which have high performance thanks to a sophisticated design [57]. All light detectors were equipped with one NTD Ge thermistor.

Table 4 Information about Ge light detectors used in the present work. The detectors are grouped according to the mounting standard given in the first column

Standard	Light detector ID	Ge size (mm)	Coating	Sensor	
				NTD	mass (mg)
LUMINEU	M1	⌀44×0.17	yes	LR	20
	M3	⌀44×0.17	yes	LR	9
	Lum11	⌀44×0.17	yes	HR	5
	Lum12	⌀44×0.17	yes	HR	5
LUCIFER	GeB	⌀45×0.30	no	LR	9
	GeT	⌀45×0.30	no	LR	9
CUPID-0	GeOld	⌀45×0.300	no	LR	9
IAS	B297	⌀40×0.045	no	LR	1
	B304	⌀25×0.030	no	LR	1

3.3 Low-temperature low-background measurements

The list of the low-background bolometric experiments is given in Table 5. The measurements in the CUPID R&D set-up were rather short, not longer than one month of data taking, while considerably longer investigations were achieved in the EDELWEISS-III set-up. Another difference is related to the temperature conditions which were significantly colder in the CUPID R&D cryostat. Apart from two measurements, most of the data were acquired at 1 kSPS. Bias currents of the order of a few nA were set to maximize the signal-to-noise ratio resulting in a working-point thermistor resistance of a few MΩ.

Scintillating bolometers in the EDELWEISS-III cryogenics facility were operated together with high-purity Ge 800-g FID hybrid bolometers (Fully Inter-Digitized electrode design; 20–36 detectors in each cryogenic run). The ZMO-b bolometer was chosen as a reference detector and studied in all measurements at LSM described here; most results of Run308 obtained with this detector are published in [23, 24, 25]. In particular, the ZMO-b bolometer was devoted in Run310 to test the detector mechanical decoupling system — introduced for the first time in that occasion — and to compare its reference performance with that of the first $Li_2{}^{100}MoO_4$ detector (enrLMO-t) operated at Modane.

3.4 Data analysis

An optimum filter technique [58, 59] was used to evaluate the pulse height and shape parameters. It relies on the knowledge of the signal template and noise

Table 5 General information about measurements with Mo-containing bolometers operated at Modane or Gran Sasso underground laboratories. T_{base} denotes the base temperature

Set-up	Run ID	Detectors ID		Sampling (kSPS)		T_{base} (mK)	Data taking (h)
		Heat	Light	Heat	Light		
EDELWEISS-III	Run308	ZMO-t ZMO-b	M1 M3	1	1	18	5000
	Run309	ZMO-b	M3	1	1	20	2966
	Run310	ZMO-b enrLMO-t	Lum12 Lum11	1	1	19–20	2090
CUPID R&D		LMO-1	B297	2	2	11	328
		LMO-2 LMO-3	GeB B304	1	1	11	201
		enrZMO-t enrZMO-b	GeB GeT	1	1	11	717
		enrLMO-b	GeOld	2	4	12	487

power spectrum; both are estimated from the data. For those detectors that were equipped with two temperature sensors, the data of the thermistor with the best signal-to-noise ratio were analyzed. The light-detector signal amplitude is estimated at a fixed time delay with respect to the heat signals as described in Ref. [60]. The filtered amplitudes of the signals from the main crystal are corrected for the shift in thermal gain due to spontaneous temperature variations by means of the heater events. The heater was absent in the major part of the Run308 data, therefore for this purpose we used α events of ^{210}Po from residual crystal contamination. This approach gives results similar to the heater-based stabilization method [23].

The heat response of the scintillating bolometers is calibrated with the most intense γ lines of ^{232}Th and ^{40}K or/and ^{133}Ba sources. The light detectors, provided with the ^{55}Fe source, were calibrated with the ^{55}Mn X-ray doublet (5.9 and 6.5 keV).

4 Performance of Mo-containing scintillating bolometers

4.1 Time profile of the pulses

As one can see from Table 6, all heat channels, except $Zn^{100}MoO_4$, demonstrate pulse-shape time constants typical for massive bolometers: tens of ms for the rise time and hundreds of ms for the decay time. Both enriched $Zn^{100}MoO_4$ bolometers, the largest of all tested crystals, have a faster response, which is similar to the small ($\sim$60 g each) $Zn^{100}MoO_4$ detectors [33] and with the same behavior (twice faster signals for the bottom crystal). It should be noted that these parameters strongly depend on the detector coupling to the heat bath and on the base temperature. However, all samples tested in the CUPID R&D cryostat were cooled down to similar temperatures. In addition, massive bolometers should not exhibit the same time features of small-size detectors due to their much higher heat capacity. The fast response of the enriched $Zn^{100}MoO_4$ detectors has therefore no clear explanation and it may be due to the lower quality of the crystals. Anyway, this feature can lead to a better capability to discriminate random coincidences by heat pulse-shape analysis than that considered in Refs. [36, 37].

Table 6 Characteristics of Mo-containing scintillating bolometers. The pulse-shape time constants are the rise (τ_R) and decay (τ_D) times defined as the time difference between the 10% and the 90% of the maximum amplitude on the leading edge and the time difference between the 90% and the 30% of the maximum amplitude on the trailing edge, respectively. The signal sensitivity is measured as the thermistor voltage change for a unitary energy deposition. The intrinsic energy resolution (FWHM baseline) is determined by noise fluctuations at the filter output. The energy resolution (FWHM) of light detectors was measured with ^{55}Fe X-ray source. Some light detectors for which the baseline noise is marked by * were roughly calibrated by scintillation light (see details in the text). The FWHM resolution of heat channels is obtained for γ quanta of ^{40}K, ^{133}Ba, and ^{232}Th γ sources. LY_α and $LY_{\gamma(\beta)}$ denote light yields for α's and $\gamma(\beta)$'s, respectively. The quenching factor for α particles QF_α and the discrimination power $DP_{\alpha/\gamma(\beta)}$ are calculated according to the formulas given in the text

Scintillating bolometer	Heat detector Light detector	ZMO-b M3	 Lum12	enrZMO-t GeB	enrZMO-b GeT	LMO-1 B297	LMO-2 GeB	LMO-3 B304	enrLMO-t Lum11	enrLMO-b GeOld
Pulse-shape time constant (ms)	Light τ_R	5.2	4.6	2.4	2.9	2.3	4.0	2.7	3.5	5.1
	Light τ_D	23	24	12	14	2.6	8.5	6.4	13	13
	Heat τ_R	19	38	9.6	6.4	17	29	30	27	18
	Heat τ_D	200	204	37	18	67	339	414	169	88
Sensitivity (nV/keV)	Light signal	2200	2500	1047	1053	4030	850	15800	1900	2910
	Heat signal	48	26	73	39	166	11	23	32	89
Light FWHM (eV)	Baseline	$\sim$140*	$\sim$60*	$\sim$490	$\sim$230	$\sim$42	$\sim$420	$\sim$18	$\sim$70*	$\sim$140
	X-ray, 5.9 keV	–	–	787(3)	289(1)	334(4)	555(5)	504(4)	–	303(2)
Heat FWHM (keV)	Baseline	$\sim$1.6	$\sim$3.6	$\sim$2.6	$\sim$4.3	$\sim$0.6	$\sim$2.3	$\sim$1.6	$\sim$1.2	$\sim$1.2
	γ, 356 keV	3.7(1)	5.1(1)	–	–	–	–	–	2.54(4)	–
	γ, 911 keV	4.4(7)	10(1)	5.6(7)	9(2)	2.0(3)	3.9(6)	3.1(6)	3.1(5)	3.1(2)
	γ, 1461 keV	–	7.9(2)	6.7(6)	14(1)	–	4.2(3)	4.4(3)	4.1(2)	–
	γ, 2615 keV	9(1)	12(1)	9.1(7)	22(2)	3.8(6)	6(1)	4.7(7)	6.3(6)	5.0(5)
	α, 5407 keV	8.8(1)	9.0(2)	$\sim$47	$\sim$100	7(2)	9(1)	9(2)	5.4(3)	–
Response to $\gamma(\beta)$ and α	$LY_{\gamma(\beta)}$ (keV/MeV)	–	–	1.32	1.20	0.69	0.99	0.12	–	0.77
	LY_α (keV/MeV)	–	–	0.22	0.15	0.16	0.20	0.02	–	0.15
	QF_α	0.15	0.17	0.17	0.13	0.23	0.20	0.17	0.22	0.19
	$DP_{\alpha/\gamma(\beta)}$ (above 2.5 MeV)	12	21	7.8	11	16	8.7	11	18	12

4.2 Voltage sensitivity

A signal pulse height of the order of few tens to hundred nV/keV is typical for NTD-instrumented massive bolometers. This figure corresponds to what is observed in all the tested scintillators (Table 6). Only the LMO-1 detector exhibits a higher sensitivity, which led to an enhanced signal-to-noise ratio.

4.3 Energy resolution

The ZMO-b scintillating bolometer has shown high energy resolution over all the runs in which it was operated; the best results were obtained at the coldest base temperature (Table 6). As it is seen in Table 6, we did not get an improvement of the ZMO-b heat-channel performance by using the decoupling system because this detector was not strongly affected by vibrations in the past measurements and, in addition, the run with the suspended tower was characterized by a slightly warmer operation temperature.

The ZMO-t bolometer was affected by a signal-to-noise ratio worse by a factor 2 with respect to its twin ZMO-b in Run308. It was ascertained, by inspection of the assembly after the run conclusion, that the crystal was loosen in its holder due to insufficient tightening of the PTFE elements. Therefore, we omit quoting the ZMO-t performance in Table 6.

A dependence of the performance on the sample position in the boule is observed in the case of the $Zn^{100}MoO_4$ detectors, which is similar to the results of the small $Zn^{100}MoO_4$ scintillating bolometers test [33]: the detectors made of the top parts of the crystal boules have shown higher performance. It can be explained by better quality of the top crystal. It is also worth noting that the noise conditions were the worst among all the here-described measurements done at LNGS (as one can notice in Table 6). However, the achieved energy resolution of the $Zn^{100}MoO_4$ bolometers (e.g. illustrated for enrZMO-t in Fig. 4) is acceptable for the demonstration of the technology feasibility for the CUPID project (see in [56]).

The energy resolution of the enrLMO-t detector is the best achieved with LUMINEU detectors ever tested in the EDELWEISS set-up. Moreover, it is twice better than that obtained with the best-performance detector ZMO-b. Thanks to the colder experimental conditions and four times longer calibration measurements, the enrLMO-b detector operated in the CUPID R&D cryostat demonstrates slightly better energy resolution, which is similar to the performance of natural Li_2MoO_4 detectors operated in the same set-up, as it is seen in Table 6. The energy spectrum measured by the $Li_2{}^{100}MoO_4$ detector enrLMO-b with ^{232}Th γ source is presented in Fig. 4(a). The improvement of the intrinsic energy resolution (in comparison to the aboveground test [32]) was obtained thanks to the lower base temperature of LMO-1 (resulting in a higher signal amplitude) and reduced noise of the cryogenic environment. The energy resolution achieved with Li_2MoO_4-based cryogenic detectors (Table 6) is at the level of the best resolutions obtained with massive bolometers [9, 61].

By fitting the energy-dependance of the energy resolution for the heat channel, one can extract the expected FWHM at the $Q_{\beta\beta}$ value of ^{100}Mo, as it is illustrated in Fig. 4(b). The chosen data of $Zn^{100}MoO_4$ (enrZMO-t) and $Li_2{}^{100}MoO_4$ (enrLMO-b) detectors represent the typical energy resolution for bolometers based

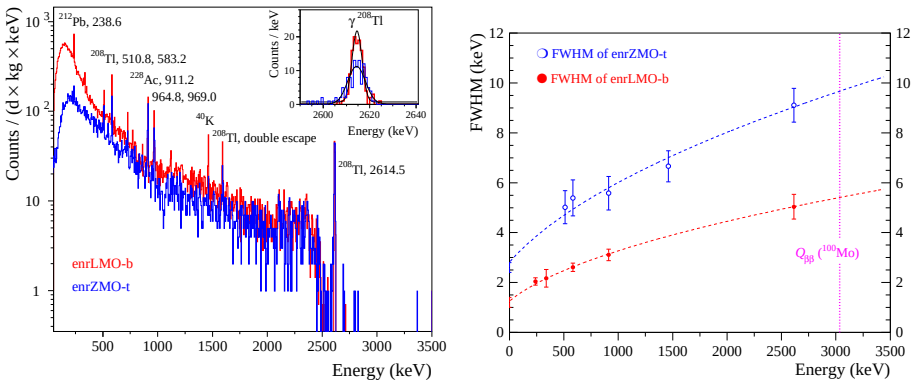

(a) (b)

Fig. 4 The energy spectra of the ^{232}Th γ source measured by the $\sim$ 0.4 kg $Zn^{100}MoO_4$ (enrZMO-t) and 0.2 kg $Li_2{}^{100}MoO_4$ (enrLMO-b) bolometers over 64 h and 168 h, respectively, at LNGS (a). The energy bin is 5 keV. (Inset) The 2615 keV peak of ^{208}Tl γ quanta accumulated by the detectors together with the fit. The energy resolution (FWHM) of the enrZMO-t (blue histogram) and enrLMO-b (red histogram) bolometers is 9 keV and 5 keV, respectively. The energy dependence of the energy resolution of the ZMO-t and LMO-b detectors (b). The fits to the data by a function FWHM (keV) $= \sqrt{(p_1 + p_2 \times E_\gamma(keV))}$ (p_1 and p_2 are free parameters) are shown by the dashed lines. The dotted line indicates the $Q_{\beta\beta}$ value of ^{100}Mo (3034 keV)

on these materials in case of optimal experimental conditions (Table 6). Using the fitting parameters for the curves shown in Fig. 4(b), the expected energy resolution of the enrZMO-t and enrLMO-b cryogenic detectors at $Q_{\beta\beta}$ of ^{100}Mo is 9.7$\pm$1.0 keV and 5.4$\pm$0.4 keV, respectively, and, in case of $Li_2{}^{100}MoO_4$, it already matches the requirements for future generation $0\nu2\beta$ experiments [7,8,9,11].

4.4 Performance of the light detectors

In contrast to the massive bolometers, light detectors have a reduced heat capacity because of the low mass of the Ge absorber — of the order of a few grams — and the small-size NTD thermistors (e.g. compare NTD mass in Tables 3 and 4). Therefore, they have significantly faster signals (just few ms rise and ten(s) ms decay times), higher sensitivity ($\sim$1–2 μV/keV) and lower baseline noise ($\sim$0.1–0.4 keV FWHM), as it is seen in Table 6. The only exceptions are the extraordinary performance of the IAS optical bolometers. However, the latter exhibit a strong position-dependent response, therefore the energy resolution measured with an uncollimated ^{55}Fe source is near to the obtained with other light detectors (FWHM $\sim$ 0.3–0.8 keV at 5.9 keV).

In order to estimate the sensitivity and the resolution of the baseline noise of the light detectors operated in the EDELWEISS-III set-up, we roughly calibrated them by using the heat-light data of ^{232}Th runs assuming that the light yield (see Sec. 4.5) for $\gamma(\beta)$ events is equal to 1.0 and 0.77 keV/MeV for $ZnMoO_4$

and $Li_2{}^{100}MoO_4$ detectors, respectively (see Table 6). It is also worth noting a dramatic improvement of the light-channel performance in the suspended tower, particularly in terms of long-term stable operability (see the next Section).

4.5 Response to α particles and scintillation-assisted particle identification

Typically, the amount of light emitted by an oxide scintillator for α particles is quenched to $\approx 20\%$ with respect to γ quanta (β particles) of the same energy (see e.g. in Ref. [18]). Thanks to this feature, the $ZnMoO_4$ and Li_2MoO_4 scintillating bolometers have shown an excellent particle identification capability, an efficient tool for the background rejection [13]. A discussion of several relevant peculiarities observed in the data of some detectors follows below.

The particle identification capability of the $ZnMoO_4$ detectors in Run308 and Run309 was affected by the vibration noise resulting into not precisely evaluated light-signal amplitudes, especially for the events with a low scintillation signal (α events and $\gamma(\beta)$'s below ~ 1 MeV). This effect is apparent in Fig. 5(a). A significant improvement in the light-detector performance — thanks to the mechanically isolated system of the suspended tower — is clearly appreciable in Fig. 5(b).

The stable and reliable light-channel performance in Run310 helped us to confirm that some α events with more quenched light output and enhanced heat signals for both ZMO-t and ZMO-b detectors (a major part of such events is distributed close to ^{210}Po, an α structure at around 6 MeV in electron energy) are not an artifact caused by noisy data processing but a real response of the $ZnMoO_4$ bolometers, probably related to the imperfection of crystals. Therefore, a bump on the right side of the ^{210}Po α peak, which was not well-understood in case of the heat signals only analysis [23, 25] can be explained by these events.

Similar but more pronounced anomalies in the response to α interactions were observed with large (e.g. see in Fig. 5(c)) and small [63] $Zn^{100}MoO_4$ detectors. Taking into account that these effects are neither visible for $\gamma(\beta)$'s nor for external α's from the smeared α source, they take place locally inside the crystal and only for particles characterized by a short-range interaction, like α's. Therefore, the expected $0\nu2\beta$ signal could not be affected. However, negative effects are expected on the precision of the α spectroscopy, which is important not only for the radiopurity determination to build a background model, but also for the off-line rejection of α-β delayed events from decays of ^{212,214}Bi-^{208,210}Tl [7, 13, 20].

The light-vs-heat data of several scintillating bolometers contain α events with energies $\sim$2–7 MeV with enlarged light signal amplitude (this is clearly visible in the data of the ZMO-b, enrZMO-b, enrLMO-t, and enrZMO-b detectors; e.g. see in Fig. 5). Most of them are originated by the scintillation properties of the reflecting film as it was confirmed by a dedicated test using a photomultiplier and an α source. A scintillation of the 3M film at the level of 15%–34% relatively to NE102A plastic scintillator (depending on the side of the film facing the photomultiplier) was observed. Such a feature spoils the particle discrimination capability of the detector for surface events. Therefore, we are going to omit the reflecting film or utilize reflecting material without scintillation in the CUPID-0/Mo demonstrator. Preliminary results of the ongoing Run311 in the EDELWEISS-III set-up, in which both $Li_2{}^{100}MoO_4$ detectors are operated without the reflecting foil, confirm the ability of the α particle discrimination at the required level in spite of a twice

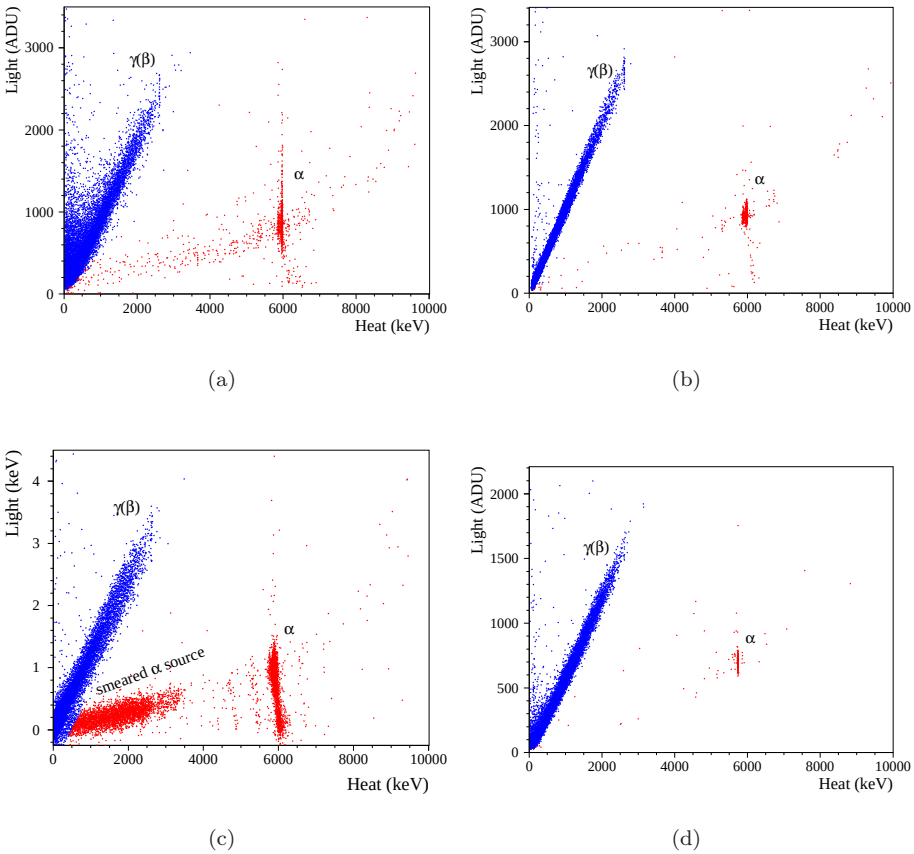

Fig. 5 Scatter plots of light versus heat signals of the background data collected with scintillating bolometers based on 334 g $ZnMoO_4$ (a and b), 382 g $Zn^{100}MoO_4$ (c), and 186 g $Li_2{}^{100}MoO_4$ (d) crystals over 2767, 1300, 593, and 1303 h, respectively. The $Zn^{100}MoO_4$ detector was operated in the CUPID R&D cryostat, other data were accumulated in the EDELWEISS-III set-up (the light signals of the later are in ADU, analog-to-digit units). The heat channels were calibrated with γ quanta and it leads to the heat miscalibration for α particles (typical for scintillating bolometers, e.g. see in Ref. [62]). The particle identification capability of the $ZnMoO_4$ detector affected by vibration noise (a) was substantially improved in the suspended tower (b). The data of all detectors contain three clear populations: β/γ events, a bunch of events due to α decays of the U/Th daughters (mainly ^{210}Po) in the crystals, energy-degraded α events caused by the surface contamination of the detectors (a, b, d) or by the external smeared α ^{238}U source (c). Events which correspond to none of these three populations are discussed in the text

reduced light collection. Moreover, escapes of nuclear recoils in alpha decays occurring at the crystal surface can be registered by a corresponding light detector leading also in this case to the enlargement of the light signal for α's (it is often observed for a typical surface pollution of $ZnMoO_4$ and Li_2MoO_4 crystals by ^{210}Po, as it is seen in Fig. 5). Thus, there is an additional argument to draw a considerable attention to crystal surface purity (see Sec. 5.3), taking also into account that a significant part of the background in the ROI of a next-generation bolometric

$0\nu2\beta$ experiment is expected to be originated at the surface of a detector and close materials [9, 26].

The commonly used particle identification parameter for scintillating bolometers is the light yield, defined as a ratio of the light signal measured in keV to the heat signal measured in MeV. The LY values for $\gamma(\beta)$ and α events obtained from the data of all investigated detectors are given in Table 6. We are not able to give the LY values in the convenient keV/MeV unit for the data accumulated in the EDELWEISS-III set-up due to the lack of light channel calibration. The measured light yields for both $Zn^{100}MoO_4$ scintillating bolometers are similar to those in previously investigated natural and ^{100}Mo-enriched $ZnMoO_4$ detectors (e.g. see [20, 30, 33]). Thanks to the progress in the development of lithium molybdate scintillators — as documented in the present work and recently in Ref. [42] — the LY values for Li_2MoO_4 and $Li_2{}^{100}MoO_4$ scintillation bolometers become comparable to the light yields of the $ZnMoO_4$-based detectors. The improvement of LY with respect to early investigations with Li_2MoO_4 detectors [21, 22] is of about a factor two. The LMO-3 bolometer was viewed by a light detector with a significantly lower area implying a reduced light collection and consequently rather small LY values. It is worth noting that $LY_{\gamma(\beta)} \sim 0.1$ keV/MeV for $\gamma(\beta)$ events does not allow effective particle identification by using a standard-performance light detector (this is the case for Cherenkov light tagging in TeO_2 bolometers; e.g. see Ref. [64] and references therein). However, the performance of the IAS optical bolometer — which featured 18 eV FWHM baseline noise — was high enough to provide highly-efficient particle identification with this detector.

The ratio of the LY parameters for α's and $\gamma(\beta)$'s gives the quenching factor of the scintillation light signals for α particles: $QF_\alpha = LY_\alpha/LY_{\gamma(\beta)}$. The QF_α can be also estimated for the non-calibrated light channel data, because light signals of both $\gamma(\beta)$ and α events of a certain detector are measured in the same set-up. As it is seen in Table 6, the results for $ZnMoO_4$ and Li_2MoO_4 detectors are similar.

Efficiency of discrimination between α and $\gamma(\beta)$ events can be characterized by the so-called discrimination power $DP_{\alpha/\gamma(\beta)}$ parameter. According to [9], we define this parameter at a certain energy E as:

$$DP_{\alpha/\gamma(\beta)} = (\mu_{\gamma(\beta)}(E) - \mu_\alpha(E))/\sqrt{\sigma^2_{\gamma(\beta)}(E) + \sigma^2_\alpha(E)},$$

where μ (σ) denotes the average value (width) of the α or $\gamma(\beta)$ distribution. The $DP_{\alpha/\gamma(\beta)}$ value is estimated for $\gamma(\beta)$ and α events selected in the energy range 2.5–2.7 MeV and 2.5–7 MeV, respectively. The interval for the selection of α's is reduced to 2.5–3.5 MeV for the measurements performed with a smeared α source. All the results are listed in Table 6 and demonstrate a high level of the $\alpha/\gamma(\beta)$ discrimination (more than 99.9% α rejection while preserving practically 100% $0\nu2\beta$ signal detection efficiency).

4.6 Response to neutrons

The ZMO-b, LMO-1, and enrLMO-t detectors were also exposed to neutrons from an AmBe source. The results for Li-containing bolometers are illustrated in Figs. 6 and 7(a). The $\gamma(\beta)$ band exceeds the natural ^{208}Tl end-point because of the prompt de-excitation γ's following ^{9}Be(α,n)^{12}C* reaction. The cluster of events in the α

region is caused by the reaction ^{6}Li(n,t)α. The ^{6}Li has a natural abundance of 7.5%, and the large cross section for thermal neutrons gives rise to the clear line at a heat energy of around 5 MeV. Due to the calibration by γ quanta, the distribution is shifted of about 7% with respect to the 4.78 MeV total kinetic energy released in the reaction. The energy resolution (FWHM) on the thermal-neutron capture peak was 7.7(3) and 5.9(2) keV for the LMO-1 and enrLMO-t detectors, respectively. This is an unprecedented high energy resolution obtained with ^{6}Li-containing detectors (e.g. compare with the results of Li-containing cryogenic detectors in Refs. [22,65,66] and references therein). A second structure at higher energy is attributed to the non-thermalized neutrons, in particular to the resonant absorption of 240 keV neutrons. A linear fit to the less prominent lower band, ascribed to nuclear recoils induced by fast neutron scattering, gives $LY = 0.07(2)$ keV/MeV. The difference in the quenching for α and nuclear recoils events is expectable [18,66].

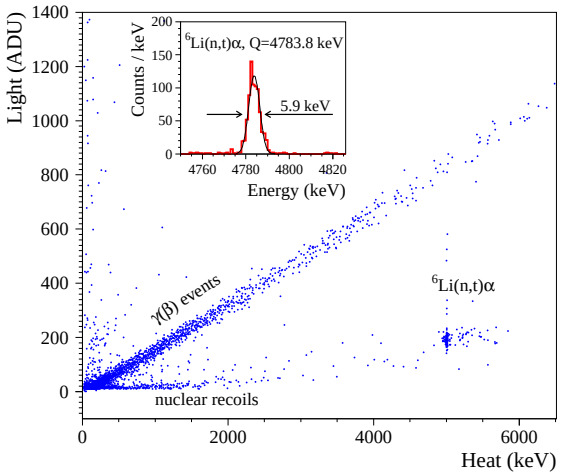

Fig. 6 The light versus heat data accumulated with the 186 g $Li_2{}^{100}MoO_4$ scintillating bolometer (enrLMO-t) in the EDELWEISS-III set-up (21–20 mK data) under neutron irradiation of an AmBe neutron source (21(4) n/s) over 33.5 h. Three populations ascribed to $\gamma(\beta)$'s, α+^{3}H events and nuclear recoils due to neutron scattering are well separated. (Inset) The ^{6}Li thermal neutron capture peak (calibrated in alpha energy) together with the Gaussian fit. The energy resolution is FWHM = 5.9 keV

4.7 Particle identification by heat signals

Previous measurements with $ZnMoO_4$ detectors demonstrated a possibility of pulse-shape discrimination by using only the heat channel [8,19,55]. However, the discrimination ability strongly depends on the experimental conditions and sometimes can fail [67]. No indication of this possibility has been claimed yet for Li_2MoO_4 bolometers.

A tiny difference between α and $\gamma(\beta)$ heat pulses of the enrZMO-t detector allows us to perform an event-by-event particle identification using only the heat

signals (e.g. $DP_{\alpha/\gamma(\beta)} = 3.8$ was obtained for 2.5–3.5 MeV data). The data of the enrZMO-b bolometer, more affected by noise, show partial particle identification ability by means of the heat channel. It is worth to note that these results were obtained in spite of a low sampling rate (1 kSPS).

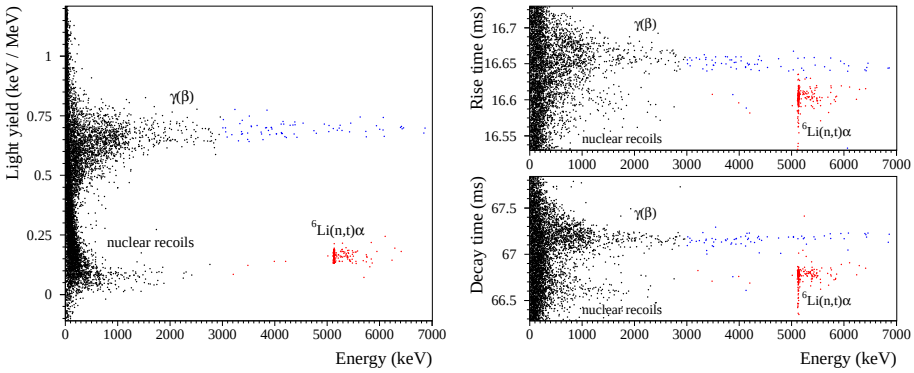

(a) (b)

Fig. 7 Light-vs-heat scatter-plot obtained in a 20.5 h AmBe (∼100 n/s) calibration measurement with a 151 g Li_2MoO_4 scintillating bolometer (a). Rise (top panel) and decay (bottom panel) times as functions of the energy (b). The populations of $\gamma(\beta)$ and ^{6}Li(n,t)α events used for the evaluation of the discrimination power are marked blue and red, respectively

The data acquired with Li_2MoO_4-based cryogenic detectors also demonstrate a possibility of the pulse-shape discrimination by the heat-signal shape analysis. This remarkable feature has been clearly shown by the LMO-1 detector (2 kSPS data). As an example, the rise and decay time parameters of the heat signals as a function of the energy are shown in Fig. 7 (b). We evaluate a $DP_{\alpha/\gamma(\beta)}$ of 5.7 and 8.2 at the α-triton peak energy by exploiting the rise and decay time parameters, respectively. The $\alpha/\gamma(\beta)$ separation achieved by the heat-signal shape analysis is clearly visible in the LMO-2 data too, which also allows to compare the signals of two populations at the same energy scale. However, the applied sampling frequency is not optimal to fully profit from the tiny difference in time constants of $\gamma(\beta)$ and α heat pulses (less than ∼0.5 ms, i.e. half of a bin for the 1 kSPS sampling). The heat data of the enrLMO-b detector, acquired with 2 kSPS rate, also provides a reasonable event-by-event particle identification with the heat channel. Unfortunately, we do not have large statistics of both types of radiation in the same energy range to investigate this feature more precisely.

5 Backgrounds and radiopurity of Mo-containing scintillating bolometers

5.1 Gamma(beta) background

5.1.1 $\gamma(\beta)$ background below 2615 keV

The background spectra of $\gamma(\beta)$ events measured by the ZMO-b detector in the Run308–310 are shown in Fig. 8. The data acquired at different positions of the detector inside the cryostat are almost similar. Few γ peaks present in the spectra are caused by a residual contamination of the set-up [68] or/and the detector components by K, Th and U. The isotope of ^{100}Mo is present in natural molybdenum at the level of 9.7% [69], therefore the $2\nu2\beta$ decay of this nucleus gives a dominant background above 1.5 MeV even for the natural $ZnMoO_4$ detector (see Fig. 8).

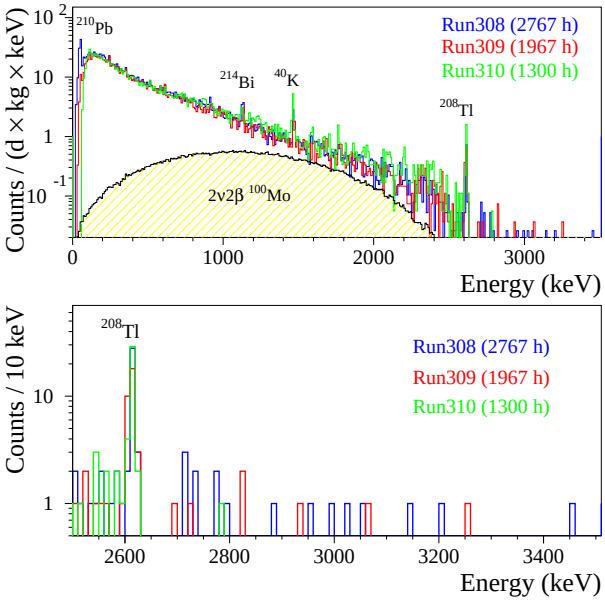

Fig. 8 The normalized energy spectra of $\gamma(\beta)$ events accumulated in the low-background measurements with the 334 g $ZnMoO_4$ scintillating bolometer in the EDELWEISS-III set-up. Monte Carlo simulated energy spectrum of the $2\nu2\beta$ decay of ^{100}Mo with the half-life $T_{1/2} = 6.90 \times 10^{18}$ yr (measured in the present work, see Sec. 5.1.3) is shown (upper panel). The energy bin is 10 keV. The same data in the 2.5–3.5 MeV energy interval (lower panel)

The $\gamma(\beta)$ background accumulated by three Li_2MoO_4 detectors in the CUPID R&D set-up is shown in Fig. 9. The region below 1.5 MeV of the LMO-1 detector is dominated by ^{40}K due to potassium contamination of the crystal. The main ^{40}K decay mode (branching ratio BR = 89.3% [70]) is the β^- decay with Q_β = 1311 keV [71]. The 1460.8 keV de-excitation γ-quanta following the ^{40}K electron capture in ^{40}Ar* (BR = 10.7%; K-shell electron binding energy is 3.2 keV) is also clearly visible with a total energy of 1464 keV. The ^{208}Tl γ peak in the LMO-1

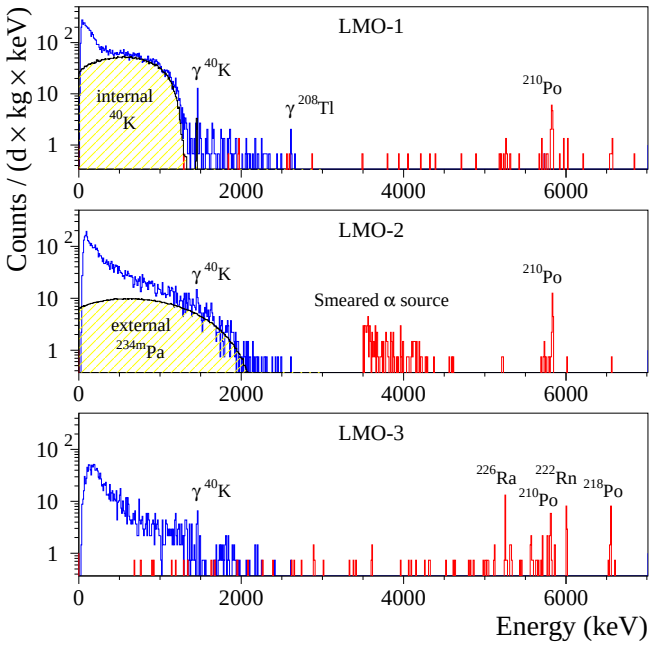

Fig. 9 The background energy spectra measured with the LMO-1 (over 237.5 h, upper panel), LMO-2 (135 h, middle panel) and LMO-3 (135 h, lower panel) scintillating bolometers. The energy bin is 10 keV. The α events in red are selected with the help of the light-heat cut (the events of the ^{238}U smeared α source for the LMO-2 detector are not shown below 3.5 MeV). An internal potassium contamination of the LMO-1 crystal generates the continuum up to $\approx$ 1.3 MeV and the γ de-excitation peak at 1464 keV. The ^{208}Tl line visible in the LMO-1 data can be ascribed to the thorium contamination of the set-up. The β spectrum of ^{234m}Pa in the LMO-2 detector is due to the smeared ^{238}U α source. The α peaks of ^{210}Po (common for all the crystals) and ^{226}Ra with daughters (in LMO-3) are caused by the residual contamination of the Li_2MoO_4 crystals

data is due to the thorium contamination of the set-up. The $\gamma(\beta)$ backgrounds of the LMO-2 and LMO-3 detectors contain only the ^{40}K peak caused by the potassium contamination of the set-up. The ^{40}K activity in the LMO-1 and the limits for LMO-2 and LMO-3 crystals are given in Table 7.

As one can see in Fig. 10(a), the energy spectra of $\gamma(\beta)$ events measured by both $Zn^{100}MoO_4$ bolometers are rather similar; the main difference is related to the better energy resolution of the enrZMO-t detector. In spite of the different background conditions in the set-ups located at different underground sites, the $\gamma(\beta)$ spectra accumulated by the $Li_2{}^{100}MoO_4$ bolometers are also very similar above 1 MeV, as it is seen in Fig. 10(b). This is explained by the fact that the counting rate of all the ^{100}Mo-enriched detectors above 1 MeV is dominated by the $2\nu2\beta$ decay of ^{100}Mo with an activity of $\sim$10 mBq/kg. The excess of events below 0.8 MeV for the enrLMO-b data indicates a higher external background in the CUPID R&D cryostat in comparison to the EDELWEISS-III set-up.

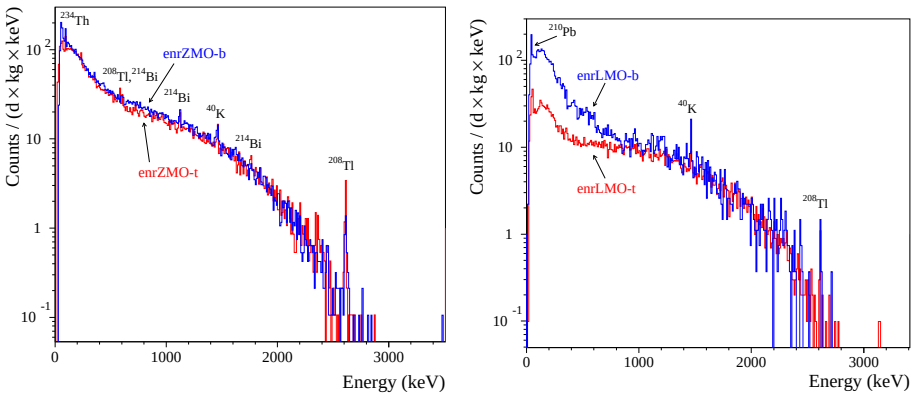

(a) (b)

Fig. 10 The energy spectra of $\gamma(\beta)$ events measured by the $\sim$ 0.4 kg $Zn^{100}MoO_4$ (a) and $\sim$ 0.2 kg $Li_2{}^{100}MoO_4$ (b) scintillating bolometers. The energy bin is 10 keV. The data of both $Zn^{100}MoO_4$ and one $Li_2{}^{100}MoO_4$ (enrLMO-b) detectors were accumulated in the CUPID R&D cryostat, while the enrLMO-t bolometer was measured in the EDELWEISS-III set-up. The origin of the most intensive γ peaks is denoted

5.1.2 $\gamma(\beta)$ background above 2615 keV

There is an indication of the counting-rate decrease above the energy 2615 keV in the ZMO-b detector (see Fig. 8): the counting rate of events in the 2.65–3.5 MeV energy range was 0.14(3), 0.08(3), and 0.02(2) cpd in Runs 308, 309, and 310, respectively. The decrease can be explained by a cosmogenic activation of the crystal, which was investigated with the help of COSMO [72] and ACTIVIA [73] codes, which gave compatible results. The exposure period of the ZMO-b crystal before Runs 308 and 310 was similar (around 60 days); the main difference is an 8 h air shipment, which can give an activation comparable to the sea-level exposure [74]. The crystal had a long cooling-down period, i.e. around 1.8 year including Runs 308 and 309. Only a few long-lived cosmogenic radionuclides (or their daughters) with Q-values above 3 MeV can be produced in $ZnMoO_4$ with a comparatively high production rate $\geq$0.01 decays/kg/d: ^{56}Co, ^{82}Rb(^{82}Sr) and ^{88}Y(^{88}Zr). After 60 days exposure at sea level, their estimated activities are at the level of 0.01 mBq/kg and the expected total background rate in the 2.65–3.5 MeV energy interval for Run308 is below 0.03 cpd, which is lower than that the measured rate. The counting rate above 2615 keV cannot be explained by internal thorium contamination of the crystal: the ^{228}Th activity in the ZMO-b scintillator is limited on the level of 4.6 μBq/kg (see [23] and Table 7). Taking into account that a considerable part of γ background of the EDELWEISS-III set-up originates from radioactive contamination of the Delrin® BeCu connectors [68] (placed on the external lateral surface of the detector holders), coincidences of ^{208}Tl γ's can produce events above 2615 keV. Indeed, the Monte Carlo simulations of a close point-like Th source show that the total number of events in the 2.65–3.5 MeV range corresponds to approximately half of the area of the 2615 keV peak. This is

compatible with the results of Runs 308 and 309, but in disagreement with those of Run310. The muon events are not considered in the present data, however they cannot provide the observed excess of high energy events. In addition, the higher surface purity of the ZMO-b detector in Run310 should lead to a lower rate of surface-induced $\gamma(\beta)$ events [9]. So, the background sources considered separately cannot explain the measured rate above 2615 keV and, therefore, a detailed Monte Carlo simulations and new measurements with other detectors are in progress to understand this background.

Also the data from the $Zn^{100}MoO_4$ and $Li_2{}^{100}MoO_4$ detectors show a few events above the 2615 keV γ peak of ^{208}Tl (see Fig. 10). An event-by-event analysis excludes that they are due to random coincidences of $2\nu2\beta$ events. As in the case of the $ZnMoO_4$ detector, they may be caused by cosmogenic activation of the crystals, a radioactive contamination of the set-up by thorium and radium, and surface contamination of the crystals and the set-up.

5.1.3 Double-beta decay of ^{100}Mo

The low-background data of the ^{100}Mo-enriched detectors were also used to investigate the double-beta decay of ^{100}Mo.

To extract the half-life value of ^{100}Mo relative to $2\nu2\beta$ decay, the energy spectrum of $\gamma(\beta)$ events accumulated by the enrLMO-t detector was fitted by a simplified background model (Fig. 11). Taking into account a high crystal radiopurity (see Table 7), only two components of the internal background — the $2\nu2\beta$ decay of ^{100}Mo and the bulk ^{40}K decay — are expected to give a valuable contribution to the measured spectrum. The response function of the detector has been simulated with the help of the GEANT4-based code [75] and the DECAY0 event generator [76]. A model of the residual (external) background was built from an exponential function and the distributions of ^{40}K and ^{232}Th (built from the calibration data). The best fit (χ^2/n.d.f. = 259.6/240 = 1.08) obtained in the energy interval 160–2700 keV gives 8853 ± 186 decays of the $2\nu2\beta$ of ^{100}Mo and 1998 ± 605 decays of the internal ^{40}K. Taking into account the mass of the crystal (185.9 ± 0.1 g), the live time (1303.23 ± 26.06 h), and the pulse-shape discrimination efficiency (0.971 ± 0.004), the bulk activity of ^{40}K in the enrLMO-t crystal is estimated to be 2.4 ± 0.7 mBq/kg (or $\leq$3.5 mBq/kg). The enriched crystal (0.969 ± 0.002 of ^{100}Mo) contains 6.103×10^{23} nuclei of ^{100}Mo and, therefore, the $2\nu2\beta$ decay half-life of ^{100}Mo is $T_{1/2} = (6.90 \pm 0.15)\times10^{18}$ yr (statistical uncertainty only). Additional components of the systematic error are related to the Monte Carlo simulations (5%; corresponds to the uncertainty of the GEANT4 modeling of electromagnetic interactions [77]) and to the fit by the background model (2.8%). For the latter one, we made a fit with the described model in different energy intervals: the left side was varied in the 160–300 keV range with a 10 keV step, while the right side was set within the interval 2650–2750 keV with a 50 keV step. This kind of fits gave a number of ^{100}Mo $2\nu2\beta$ decays in the range of 8821–8888. Moreover, by using another model ($2\nu2\beta$ plus ^{232}Th distributions), we did a fit to the data above 1.5 MeV, where the signal-to-background ratio is expected to be rather high, 8:1. With the left side varied in the 1.5–1.8 MeV range with a 50 keV step and the aforementioned sets of the right band, we got 9014–9103 $2\nu2\beta$ decays and the highest variation was used as an estimator of the systematic error of the fit

model. The combination of all the contributions gives 6.1% of the total systematic uncertainty. So, the half-life of the $2\nu2\beta$ decay of ^{100}Mo is measured to

$$T_{1/2} = [6.90 \pm 0.15(\text{stat.}) \pm 0.42(\text{syst.})] \times 10^{18} \text{ yr}.$$

The obtained value is in a good agreement with the most accurate results achieved by NEMO-3 experiment, $[7.11 \pm 0.02(\text{stat.}) \pm 0.54(\text{syst.})] \times 10^{18}$ yr [78] and $[6.93 \pm 0.04(\text{stat.})] \times 10^{18}$ yr [79] [1], and the bolometric measurements with $ZnMoO_4$ crystals $[7.15 \pm 0.37(\text{stat.}) \pm 0.66(\text{syst.})] \times 10^{18}$ yr [67], as well as with the average value $[7.1 \pm 0.4] \times 10^{18}$ yr [5].

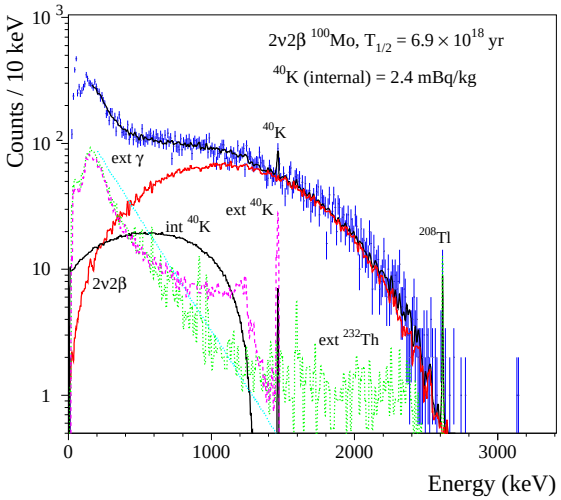

Fig. 11 The $\gamma(\beta)$ background spectrum accumulated with the 186 g $Li_2{}^{100}MoO_4$-based detector in the EDELWEISS-III set-up together with the fit by a simplified background model built from the $2\nu2\beta$ distribution of ^{100}Mo ($T_{1/2} = 6.9{\times}10^{18}$ yr), internal ^{40}K (2.4 mBq/kg bulk activity), and external γ quanta represented by exponential background (ext γ), external ^{40}K and ^{232}Th

Because of the large mass and the relatively long measurement ($\sim$ 600 h), the largest exposure was accumulated with the two $\sim$ 0.4 kg $Zn^{100}MoO_4$ detectors operated in the Gran Sasso laboratory, containing $\sim 2 \times 10^{24}$ ^{100}Mo nuclei. The usage of the smeared ^{238}U source, which also emits electrons with an end-point $\sim$ 2 MeV (see above the case of the LMO-2 detector), prevents to get more precise $2\nu2\beta$ half-life value of ^{100}Mo than that obtained from the analysis of the enrLMO-t background. However, these data were used to search for neutrinoless double-beta decay of ^{100}Mo and no counts were observed in the region of interest around 3034 keV. Considering an efficiency of $\sim$ 75% in a 10 keV energy window, we were able to set a limit on $0\nu2\beta$ decay of ^{100}Mo of 2.6×10^{22} yr at 90% C.L. Of course, this result is by far inferior to that achieved by NEMO-3 with 6.914 kg of ^{100}Mo over the live time of 4.96 yr ($T_{1/2} \geq 1.1 \times 10^{24}$ yr at 90% C.L. [79]), but — given the low sensitive mass and the short duration of the test — it represents a high potential of scintillating bolometers approach.

[1] The value of [79] is a preliminary result of the NEMO-3 Phase I+II obtained from the fitting to the data above 2 MeV; the complete analysis is ongoing.

5.2 Alpha background

The distributions of α events were selected from the background data of the tested scintillating bolometers and used to estimate the bulk radioactive contamination of the crystals. The high energy part of the α spectra (above 4 MeV), where α events of the U/Th chains occur, has been analyzed for this purpose (see [23] for details of the analysis). The area of the α peaks was determined within $\pm 3\sigma$ interval around the corresponding Q-value, while the background is estimated in the energy intervals 3.4–4 and 4.35–4.65 MeV. The σ value is taken from the results of fits to the ^{210}Po peaks observed for all detectors. In case of no clear evidence of the contamination, the Feldman-Cousins approach [80] was applied to determine, as an upper limit at 90% C.L., the maximum number of events which can be ascribed to the peak searched for.

The ZMO-b crystal radiopurity has been investigated in [23,25] using the data of Run308. Taking into account the lower rate of surface α's achieved in Run310, we used the new data to re-evaluate the radioactive contamination of the crystal. In spite of a considerably larger statistics collected with the ZMO-t detector in comparison to the most of measurements with other detectors, its sensitivity to α-active radionuclides is limited by the poor energy resolution (e.g. FHWM $\sim$ 60 keV at 5407 keV of ^{210}Po). A clear signature of the ZMO-t data is a ^{210}Po (daughter of ^{210}Pb) contamination with approximately two times lower activity than that in the ZMO-b crystal, which indicates ^{210}Pb segregation. A summary of the $ZnMoO_4$ crystals' radioactive contamination is given in Table 7.

The α spectra of the three Li_2MoO_4 detectors are shown in Fig. 9. Only the ^{210}Po peak is evident in the data accumulated with the LMO-1 and LMO-2 detectors. The LMO-3 crystal, produced from another Li_2CO_3 compound strongly polluted by ^{226}Ra, exhibits a clear ^{226}Ra contamination too. There is also a hint of a ^{226}Ra contamination of the LMO-1 and LMO-2 crystals, but the low statistics acquired does not allow us to make a strong statement. It should be also stressed that we cannot distinguish precisely a surface ^{210}Po pollution from a bulk one. Furthermore, most likely the observed ^{210}Po is due to ^{210}Pb contamination of the crystals, as it is the case for the $ZnMoO_4$ scintillator [23]. There are no other features in the Li_2MoO_4 data which can be interpreted as radioactive contamination of the detectors. Therefore, except ^{210}Po (and ^{226}Ra), we set upper limits on radioactive contamination of the crystal scintillators (see in Table 7).

The α-induced backgrounds of ^{100}Mo-enriched detectors are shown in Fig. 12. The anomalies in the response to α's of the $Zn^{100}MoO_4$ bolometers were corrected by using the results of the fit to the ^{210}Po events distribution in the LY-vs-heat data. The ^{232}Th calibration data (168 h) of the enrLMO-b detector were combined with the background data to increase the statistics. Similarly to the crystals produced from molybdenum with natural isotopic composition, the main contribution to the α spectra of all the enriched scintillators comes from ^{210}Pb contamination. The enrLMO-b detector exhibits a higher surface pollution by ^{210}Po than enrLMO-t. In contrast to the $Li_2{}^{100}MoO_4$ crystals, both $Zn^{100}MoO_4$ samples exhibit ^{238}U, ^{234}U, and ^{226}Ra contamination because of only one applied boule crystallization.

Table 7 Radiopurity of $ZnMoO_4$ and Li_2MoO_4 crystal scintillators developed from highly purified natural and ^{100}Mo-enriched molybdenum. The errors are estimated at 68% C.L., the upper limits are given at 90% C.L. The crystal masses and durations of the considered background data are also given for comparison

Chain	**Nuclide**	**Activity in μBq/kg**								
		ZMO-t	ZMO-b	enrZMO-t	enrZMO-b	LMO-1	LMO-2	LMO-3	enrLMO-t	enrLMO-b
		336 g	334 g	379 g	382 g	151 g	241 g	242 g	186 g	204 g
		1540 h	1300 h	593 h	593 h	237 h	135 h	135 h	1303 h	487 h
^{232}Th	^{232}Th	≤ 7.3	≤ 1.4	≤ 8.0	≤ 9.0	≤ 18	≤ 21	≤ 18	≤ 2.7	≤ 11
	^{228}Th	≤ 26	≤ 4.6	≤ 8.0	≤ 21	≤ 18	≤ 21	≤ 18	≤ 8.4	≤ 6.2
^{238}U	^{238}U	≤ 13	≤ 2.6	10(4)	39(7)	≤ 18	≤ 37	≤ 48	≤ 4.9	≤ 11
	^{234}U	≤ 20	≤ 3.0	11(6)	43(10)	≤ 18	≤ 21	≤ 46	≤ 6.7	≤ 11
	^{230}Th	≤ 28	≤ 1.4	≤ 17	≤ 24	≤ 18	≤ 21	≤ 18	≤ 2.7	≤ 11
	^{226}Ra	≤ 26	≤ 6.2	14(3)	23(4)	≤ 44	≤ 37	130(19)	≤ 6.7	≤ 11
	^{210}Po	575(18)	$1.32(3)\times10^3$	809(32)	$2.39(5)\times10^3$	139(33)	195(41)	76(25)	230(20)	60(10)
^{235}U	^{235}U	≤ 19	≤ 2.6	≤ 13	≤ 19	≤ 18	≤ 21	≤ 18	≤ 4.9	≤ 6.2
	^{231}Pa	–	≤ 1.4	≤ 8.0	≤ 36	≤ 18	≤ 21	≤ 18	≤ 2.7	≤ 6.2
	^{227}Th	–	≤ 2.6	≤ 8.5	≤ 12	≤ 18	≤ 21	≤ 18	≤ 4.9	≤ 6.2
	^{40}K	–	–	–	–	$62(2)\times10^3$	$\leq 12\times10^3$	$\leq 3.2\times10^3$	$\leq 3.5\times10^3$	$\leq 3.5\times10^3$
	^{190}Pt	≤ 4.4	2.6(13)	–	–	≤ 18	–	≤ 18	≤ 2.7	≤ 11

It is also evident that the top $Zn^{100}MoO_4$ crystal is less contaminated than that the bottom one confirming the segregation of ^{238}U and its daughters during the crystal growth. This effect can be used to improve further the crystal radiopurity by applying recrystallization. It is interesting to note that the higher ^{210}Po activity in the enrLMO-t indicates a depletion of impurities during the Li_2MoO_4 crystal growth process (see also [42]). Table 7 summarizes the radioactive contamination of the $Zn^{100}MoO_4$ and $Li_2{}^{100}MoO_4$ crystal scintillators. The achieved radiopurity of ^{100}Mo-enriched $ZnMoO_4$ and Li_2MoO_4 crystals satisfies the demands of a next-generation bolometric $0\nu2\beta$ experiment [7,8,9].

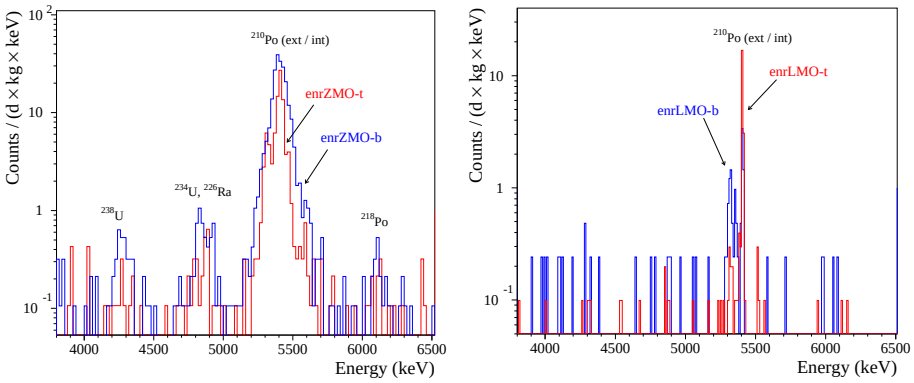

(a) (b)

Fig. 12 The energy spectra of α events detected by the 0.4 kg $Zn^{100}MoO_4$ (a) and the 0.2 kg $Li_2{}^{100}MoO_4$ (b) scintillating bolometers. The energy bin is 20 keV and 10 keV, respectively. The data of enrZMO-t and enrZMO-b (both over 593 h), and enrLMO-b (487 h) detectors were collected in the low background measurements in the CUPID R&D cryostat at LNGS. The enrLMO-t (1303 h) bolometer has been operated in the EDELWEISS-III set-up at LSM

5.3 Surface background

As one can see in Fig. 5, the detectors measured in Run310 exhibit suppressed surface contamination resulting in a lower counting rate of energy-degraded α's in comparison to the past runs. In particular, the α rate in the energy interval 2.7–3.9 MeV (excluding the region of ^{190}Pt, expected at $Q_\alpha = 3252$ keV [71]) was reduced from 0.7(1) and 0.52(6) counts/yr/kg/keV in Run308 (for ZMO-t and ZMO-b, respectively) to 0.20(6) and 0.09(5) counts/yr/kg/keV in Run310 (for ZMO-b and enrLMO-t, respectively). This purity is comparable to the Cuoricino data (0.110(1) counts/yr/kg/keV [16]) but a factor 5 worse than the purity achieved in CUORE-0 (0.016(1) counts/yr/kg/keV [17]). However, it is worth noting that no special efforts were dedicated for the surface cleaning in these prototypes of LUMINEU detectors, while a significantly reduced amount of copper

structure, a special surface treatment [81] and a dedicated mounting system [82] were adopted in CUORE-0.

5.4 Neutron background

The data acquired with the enrLMO-t and enrLMO-b detectors were used to estimate the thermal neutron flux inside the EDELWEISS-III and CUPID R&D set-ups by using the clear signature of neutron capture by ^{6}Li: an α+t event at energy of 4784 keV. The data of the enrLMO-t detector do not contain any evidence of such events (there are no events observed even in the wider energy range of 4680–4850 keV), while an event is found in the enrLMO-b data. The expected background in the region (the same to the radiopurity analysis) is 0.054 (0.24) counts for enrLMO-t (enrLMO-b). According to Ref. [80], the number of events which can be excluded at 90% C.L. is 2.39 (4.11) counts for the enrLMO-t (enrLMO-b). Assuming 100% detection efficiency for such large-volume ^{6}Li-containing detectors (e.g. see in Ref. [65]), and taking into account the total live time (1303 h / 487 h) and the surface area (85.7 cm^2 / 90.4 cm^2) of the enrLMO-t / enrLMO-b crystals, we estimate the following upper limits on the thermal neutron flux inside the EDELWEISS-III and CUPID R&D set-ups: 5.9×10^{-9} n/cm^2/s and 2.6×10^{-8} n/cm^2/s at 90% C.L., respectively.

6 Conclusions

The mass production technology of large-mass ($\sim$ 1 kg) high-optical-quality zinc and lithium molybdate scintillators from deeply purified molybdenum (including enriched in ^{100}Mo) has been developed. The excellent performance and high radiopurity of scintillating bolometers based on large-volume ($\sim$ 100 cm^3) natural and ^{100}Mo-enriched $ZnMoO_4$ and Li_2MoO_4 crystals have been demonstrated in the low-background measurements at the Modane and Gran Sasso underground laboratories.

The detectors are characterized by high energy resolution (FWHM $\approx$ 4–10 keV at the 2615 keV ^{208}Tl γ peak), which is among the best ones ever achieved with massive bolometric detectors. The exploited heat-light double read-out provides an efficient particle discrimination between β/γ and α events, which is compatible with more than 99.9% α rejection while preserving approximately 100% detection efficiency of a $0\nu2\beta$ signal. Furthermore, a possibility of pulse-shape identification by using the heat channel only is demonstrated too, which is an important step towards detector simplification for the CUPID experiment intended to operate $\sim$1000 detector modules.

The radioactive contamination of the developed crystal scintillators is very low. The activity of ^{232}Th (^{228}Th) and ^{226}Ra — the most dangerous contaminants for $0\nu2\beta$ studies — is below 10 μBq/kg (few 10 μBq/kg of ^{226}Ra in case of the single boule crystallization). The total bulk α activity of U/Th is below a few mBq/kg. The activity of ^{40}K in the most radiopure Li_2MoO_4 samples is less than 4 mBq/kg. Taking into account a high isotopic enrichment of molybdenum by ^{100}Mo (about 96%), the $\gamma(\beta)$ background of enriched detectors is dominated by the $2\nu2\beta$ decay of ^{100}Mo with an activity $\sim$ 10 mBq/kg. Therefore, even a considerably low statistics

(10 kg×d) acquired with a $Li_2{}^{100}MoO_4$ detector was enough to perform one of the most accurate measurements of the half-life of ^{100}Mo relatively to the $2\nu2\beta$ decay: $T_{1/2} = [6.90 \pm 0.15(\text{stat.}) \pm 0.42(\text{syst.})] \times 10^{18}$ yr.

The Li_2MoO_4 scintillating bolometers are found to be excellent neutron low counting detectors. Their operation in the Modane and Gran Sasso cryogenic set-ups has allowed us to set very stringent limits, on the level of $\sim 10^{-8}$ neutrons/cm^2/s, on the thermal neutron flux in the EDELWEISS-III and CUPID R&D facilities.

Lessons extracted from a four years running of the LUMINEU scintillating bolometers in the EDELWEISS-III set-up are important to extend the use of this facility, oriented to dark matter search, to the investigation of 2β decay of ^{100}Mo.

Taking into account the reproducible LTG Cz growth of large-mass, high-optical quality Li_2MoO_4 crystals, the successful results of bolometric tests and the low radioactive contamination, Li_2MoO_4-based scintillating bolometers have been chosen for a pilot cryogenic 2β experiment with ≈7 kg of enriched ^{100}Mo (CUPID-0/Mo demonstrator) to prove that the developed technology meets the CUPID requirements. A first batch of twenty ∼0.2 kg $Li_2{}^{100}MoO_4$ crystal scintillators has been produced to carry out a first phase of the experiment in the EDELWEISS-III set-up.

Acknowledgements This work is a part of the program of LUMINEU, a project receiving funds from the Agence Nationale de la Recherche (ANR, France). The development of Li_2MoO_4 scintillating bolometers was carried out within ISOTTA, a project receiving funds from the ASPERA 2^{nd} Common Call dedicated to R&D activities. This work has been funded in part by the P2IO LabEx (ANR-10-LABX-0038) in the framework "Investissements d'Avenir" (ANR-11-IDEX-0003-01) managed by the Agence Nationale de la Recherche (France), by the European Research Council (FP7/2007-2013) under contract LUCIFER no. 247115 and by the Italian Ministry of Research under the PRIN 2010-2011 contract no. 2010ZXAZK9. The group from Institute for Nuclear Research (Kyiv, Ukraine) was supported in part by the IDEATE International Associated Laboratory (LIA). F.A.D. acknowledges the support of the Université Paris-Sud. The help of the technical staff of the Laboratoire Souterrain de Modane and the participant laboratories is gratefully acknowledged. We thank the mechanical workshop of CEA/SPEC for their skillful contribution to the conception and fabrication of detector holders.

References

1. J.D. Vergados, H. Ejiri, F. Šimkovic, Int. J. Mod. Phys. E **25**, 1630007 (2016)
2. V.I. Tretyak and Yu.G. Zdesenko, At. Data Nucl. Data Tables **80**, 83 (2002)
3. S. Dell'Oro, S. Marcocci, M. Viel, F. Vissani, AHEP **2016**, 2162659 (2016)
4. A. Gando et al. (KamLAND-Zen Collaboration), Phys. Rev. Lett. **117**, 082503 (2017)
5. A.S. Barabash, Nucl. Phys. A **935**, 52 (2015)
6. O. Cremonesi, M. Pavan, AHEP **2014**, 951432 (2014)
7. J.W. Beeman et al., Phys. Lett. B **710**, 318 (2012)
8. J.W. Beeman et al., Astropart. Phys. **35**, 813 (2012)
9. D.R. Artusa et al., Eur. Phys. J. C **74**, 3096 (2014)
10. C. Arnaboldi et al., Nucl. Instrum. Meth. A **518**, 775 (2004)
11. G. Wang et al. (The CUPID Interest Group), arXiv:1504.03599 [physics.ins-det] (2015)
12. G. Wang et al. (The CUPID Interest Group), arXiv:1504.03612 [physics.ins-det] (2015)
13. S. Pirro, Phys. At. Nucl. **69**, 2109 (2006)
14. A. Giuliani, J. Low Temp Phys **167**, 991 (2012)
15. S. Rahaman et al., Phys. Lett. B **662**, 111 (2008)
16. E. Andreotti et al. (Cuoricino Collaboration), Astropart. Phys. **34**, 822 (2011)
17. K. Alfonso et al. (CUORE Collaboration), Phys. Rev. Lett. **115**, 102502 (2015)
18. V.I. Tretyak, Astropart. Phys. **33**, 40 (2010)
19. L. Gironi et al., JINST **5**, P11007 (2010)

20. J.W. Beeman et al., Eur. Phys. J. C **72**, 2142 (2012)
21. O. Barinova et al., Nucl. Instrum. Meth. A **613**, 54 (2010)
22. L. Cardani et al., JINST **8**, P10002 (2013)
23. E. Armengaud et al. (the LUMINEU and the EDELWEISS collaborations), JINST **10**, P05007 (2015)
24. D.V. Poda for the LUMINEU and the EDELWEISS Collaborations, Nucl. Part. Phys. Proc. **273–275**, 1801 (2016)
25. D.V. Poda et al., AIP Conf. Proc. **1672**, 040003 (2015)
26. F.A. Danevich et al., AIP Conf. Proc. **1686**, 020007 (2015)
27. J.W. Beeman et al., J. Low Temp. Phys. **167**, 1021 (2012)
28. D.M. Chernyak et al., Nucl. Instrum. Meth. A **729**, 856 (2013)
29. M. Mancuso et al., J. Low Temp. Phys. **176**, 571 (2012)
30. L. Bergé et al., JINST **9**, P06004 (2014)
31. D.M. Chernyak et al., Opt. Mat. **49**, 67 (2015)
32. T. Bekker et al., Astropart. Phys. **72**, 38 (2016)
33. A.S. Barabash et al., Eur. Phys. J. C **74** (2014) 3133
34. A.A. Pavlyuk et al., Proc. APSAM-92, Shanghai, China (1992), Japan (1993), p. 164
35. Yu.A. Borovlev et al., J. Cryst. Growth **229**, 305 (2001)
36. D.M. Chernyak et al., Eur. Phys. J. C **72**, 1989 (2012)
37. D.M. Chernyak et al., Eur. Phys. J. C **74**, 2913 (2014)
38. F.A. Danevich et al., Nucl. Instrum. Meth. B **336**, 26 (2014)
39. V.D. Grigorieva et al., Li_2MoO_4 crystals grown by low thermal gradient Czochralski technique, Submitted to Crystal Growth & Design
40. O. Barinova et al., Nucl. Instrum. Meth. A **607**, 573 (2009)
41. O. Barinova, S. Kirsanova, A. Sadovskiy, I. Avetissov, J. Cryst. Growth **401**, 853 (2014)
42. M. Velázquez et al., Solid State Sci. **65**, 41 (2017)
43. M.B. Chadwick et al., Nucl. Data Sheets **112**, 2887 (2011); http://www.nndc.bnl.gov/endf/
44. L. Hehn et al. (The EDELWEISS collaboration), Eur. Phys. J. C **76**, 548 (2016)
45. E. Armengaud et al. (The EDELWEISS Collaboration), Performance of the EDELWEISS-III array for the direct search of dark matter, To be submitted to JINST
46. E.E. Haller, Infrared Physics & Technology **35**, 127 (1994)
47. S. Gaertner et al., Astron. Astrophys. Suppl. Ser. **126**, 151 (1997)
48. A. Alessandrello et al., Nucl. Instrum. Meth. A **412**, 454 (1998)
49. S. Pirro, Nucl. Instrum. Meth. A **559**, 672 (2006)
50. C. Arnaboldi, G. Pessina, and S. Pirro, Nucl. Instrum. Meth. A **559**, 826 (2006)
51. C. Arnaboldi et al., Nucl. Instrum. Meth. A **520**, 578 (2004)
52. E. Andreotti et al., Nucl. Instrum. Meth. A **664**, 161 (2012)
53. M. Tenconi, Ph.D. thesis, University Paris-Sud, Orsay, France (2015)
54. M. Mancuso et al., EPJ Web Conf. **65**, 04003 (2014)
55. J.W. Beeman et al., JINST **8**, P07021 (2013)
56. D.R. Artusa et al., Eur. Phys. J. C **76**, 364 (2016)
57. N. Coron et al., Opt. Eng. **43**, 1568 (2004)
58. E. Gatti, P. Manfredi, Riv. Nuovo Cim. **9**, 1 (1986)
59. V. Radeka and N. Karlovac, Nucl. Instrum. Meth. **52**, 86 (1967)
60. G. Piperno, S. Pirro, and M. Vignati, JINST **6**, P10005 (2011)
61. D.R. Artusa et al. (CUORE Collaboration), Eur. Phys. J. C **74**, 2956 (2014)
62. C. Arnaboldi et al., Astropart. Phys. **34**, 143 (2010)
63. M. Mancuso, Ph.D. thesis, University Paris-Sud, Orsay, France (2016)
64. D.R. Artusa et al., Phys. Lett. B **767**, 321 (2017)
65. M. Martinez et al., J. Phys.: Conf. Ser. **375**, 012025 (2012)
66. J. Gironnet et al., AIP Conf. Proc. **1185**, 751 (2009)
67. L. Cardani et al., J. Phys. G **41**, 075204 (2014)
68. S. Scorza for the EDELWEISS Collaboration, AIP Conf. Proc. **1672**, 100002 (2015)
69. J. Meija et al., Pure Appl. Chem. **88**, 293 (2016)
70. M. Wang et al., Chinese Phys. C **41**, 030001 (2017)
71. M. Wang et al., Chinese Phys. C **41**, 030003 (2017)
72. C.J. Martoff, P.D. Lewin, Comp. Phys. Comm. **72**, 96 (1992)
73. J.J. Back, Y.A. Ramachers, Nucl. Instrum. Meth. A **586**, 286 (2008)
74. G. Heusser, Annu. Rev. Nucl. Part. Sci. **45**, 543 (1995)
75. V.V. Kobychev, Nucl. Phys. At. Energy **12**, 301 (2011)

76. O.A. Ponkratenko, V.I. Tretyak, Yu.G. Zdesenko, Phys. Atom. Nuclei **63**, 1282 (2000); V.I. Tretyak, in preparation
77. K. Amako et al., IEEE Trans. Nucl. Sci. **52**, 910 (2005)
78. R. Arnold et al., Phys. Rev. Lett. **95**, 182302 (2005)
79. R. Arnold et al. (NEMO-3 Collaboration), Phys. Rev. D **92**, 072011 (2015)
80. G.J. Feldman, R.D. Cousins, Phys. Rev. D **57**, 3873 (1998)
81. F. Alessandria et al., Astropart. Phys. **45**, 13 (2013)
82. E. Buccheri et al., Nucl. Instrum. Meth. A **768**, 130 (2014)